Available online at www.sciencedirect.com
SCIENCE DIRECT
Journal of Sound and Vibration 294 (2006) 706–736
JOURNAL OF SOUND AND VIBRATION
www.elsevier.com/locate/jsvi

Ground vibration generated by trains in underground tunnels

J.A. Forrest[a,*], H.E.M. Hunt[b]

[a]*Maritime Platforms Division, Defence Science & Technology Organisation, 506 Lorimer St, Fishermans Bend VIC 3207, Australia*
[b]*Department of Engineering, University of Cambridge, Trumpington Street, Cambridge CB2 1PZ, UK*

Received 4 March 2004; received in revised form 4 April 2005; accepted 3 December 2005
Available online 10 March 2006

Abstract

A popular method used to reduce vibration transmitted from underground railways into nearby buildings is floating-slab track, whereby a concrete slab supporting the two rails is mounted on rubber bearings or steel springs to isolate it from the tunnel invert. This paper adds a track model to a previously developed three-dimensional tunnel model in order to assess the effectiveness of floating-slab track. A slab beam coupled to the tunnel in the wavenumber domain, with the slab bearings represented by an elastic layer, is examined first. A second beam representing the two rails together is then coupled to the slab, and axle masses representing a train are added to the rail beam. Power-spectral densities and RMS levels of soil vibration due to random roughness-displacement excitation between the masses and the rail beam are calculated. Analytical techniques are used to minimise the computational requirements of the model. The results demonstrate the inadequacy of simple mass–spring and Winkler-beam models with rigid foundations for the assessment of the vibration-isolation performance of railway track. They suggest that the achievable insertion loss is modest and that floating the track slab may in fact cause increased transmission of vibration under certain conditions.

1. Introduction

A three-dimensional tunnel model comprising a thin cylindrical shell surrounded by an infinite soil medium is presented in a companion paper [1] as the first part of a detailed model for the calculation of ground vibration from an underground railway. The current paper completes the process by adding a track model for one type of floating-slab track. This allows vibration levels in the surrounding soil due to a train running on the track to be calculated, providing a direct measure of the vibration-isolation effectiveness of the tracks.

Many aspects of the design of railway track are discussed by Esveld [2]. Non-ballasted tracks mounted directly onto concrete slabs were introduced into underground railways in the 1960s. Slab track is several times more expensive to construct and radiates more sound than ballasted track, but requires much less maintenance (Henn [3]), an advantage underground. Many different track designs have been proposed to reduce the transmission of vibration and sound and several are described in the ORE report [4], with vibration-isolation performance gauged by a simple mass-on-a-spring argument. A popular approach for underground railways involves ''floating'' the track slab on resilient bearings of rubber, glass fibre or steel springs, to give a large

*Corresponding author. Fax: +61 3 9626 8373.
E-mail addresses: james.forrest@dsto.defence.gov.au (J.A. Forrest), hemh@eng.cam.ac.uk (H.E.M. Hunt).

0022-460X/$ - see front matter © 2006 Elsevier Ltd. All rights reserved.
doi:10.1016/j.jsv.2005.12.031

isolated mass and hence low natural frequency with theoretically large reductions in vibration transmission. Designs utilising short pre-cast slab sections include the Toronto "double-sleeper" (slabs 1.5 m long), the Eisenmann track in Munich and Frankfurt (3.4 m long) and the New York subway (7 m long), while the British VIPACT system supports a continuous slab. A very large isolated mass can be achieved with composite track consisting of a floating concrete tray containing ballasted track. Examples include the Üderstadt track in Cologne, and the Barbican (two tracks on one deck) and Piccadilly Line (single-track deck) systems in London.

Design predictions of track vibration-isolation performance have often been based on a simple lumped mass–spring argument. Using this approach, Zach and Rutishauser [5] claim that a 25 dB reduction in transmitted vibration at 50 Hz can be achieved by using a floating-slab track with an 8–9 Hz natural frequency. Wettschureck and Kurze [6] use a one-dimensional impedance model for ballast mats in underground railways, assuming that the ballast mat is a simple spring and the tunnel is rigid. With this and measurements they claim a 20 dB reduction of tunnel wall vibration. Similarly large reductions are predicted by Wettschureck [7,8] for ballast mats in railway tracks above ground and on bridges. Wilson et al. [9] predict high reductions above 20 Hz for a floating-slab track designed for a 14–16 Hz natural frequency, but their measurements on the surface above the railway tunnel indicate only a modest reduction of 7 dB above 31.5 Hz. A lumped-parameter approach for underground railway track is also advocated by Capponi and Murray [10]. The pitfalls of this simplistic design approach are highlighted by Greer and Manning [11], who note that a lumped-parameter model on a rigid foundation is perhaps sufficient for a tunnel in hard-rock ground, but that more sophisticated approaches are required otherwise.

Variations on the Winkler beam, or beam on elastic foundation, have been widely used to model railway track, but the context has most often been ballasted track with the emphasis on track behaviour rather than ground vibration. Cai et al. [12] conduct a free-vibration analysis of a track modelled as a rail beam supported via springs on discrete crosswise sleeper beams, which rest on Winkler foundations. The track is composed of a number of single-span units characterised by an exact dynamic-stiffness approach. Cai and Raymond [13] extend this model by including an axial rail force to simulate thermal forces, and a varying sleeper Winkler stiffness to represent uneven ballast compaction. Cui and Chew [14] assess the performance of fixed-slab and floating track with discrete slabs by means of transmitted force calculated using models with rigid foundations and distributed-mass slabs subjected to stationary and moving harmonic loads.

Mead and Yaman [15] calculate the harmonic response of infinite beams on simple, transverse elastic, and general elastic periodic supports. Nordborg [16,17] applies the same idea to a rail beam on periodic sleeper-beam supports to determine its forced response as a linear combination of the free-vibration solutions. Gry and Gontier [18] also use a periodic approach to model a rail on sleepers via a generalised beam formulation. A beam model of floating-slab track is used by Samavedam and Cross [19] to evaluate vibration isolation. The model is like a double Winkler beam, comprising an infinite rail beam on railpad springs resting on an infinite slab beam on bearing springs. The tunnel floor is assumed to be rigid. Infinite double-beam periodic structures are used by Forrest [20] to model the rails supported on continuous and discrete floating slabs and then calculate the total force transmitted to the foundation with both single force inputs and multiple axle inputs. Belotserkovskiy [21] examines a harmonic force moving along infinite periodic structures representing railway track.

More realistic track models consider the non-rigidity of the underlying soil. Ono and Yamada [22] use a standard infinite rail beam on mass–spring sleepers, but the ballast and roadbed are considered elastic with an assumed pressure distribution acting over increasing area with depth. Responses to various rail–wheel irregularities demonstrate that waves propagate down into the roadbed, as well as along the track as in a Winkler model. Knothe and Wu [23] study the vertical receptance of a track model on uniform and layered half-spaces, and compare the results to those for a simpler model where ballast and subgrade are treated as a viscoelastic foundation. They find great differences between the two models for frequencies up to 250 Hz, because the half-space allows for damping due to wave propagation and for coupling between sleepers; the half-space models explain measured results much better. Kruse and Popp [24] also examine the effect on the track dynamics of wave propagation into the subsoil. Measurements of ground vibration from heavy freight trains are compared to a model comprising an infinite rail beam on discrete mass–spring sleepers resting on a three-dimensional layered medium by Jones [25] (with other simpler models) and Jones and Block [26].

A similar model but with a continuous layered beam representing the rails, rail pads, sleepers and ballast is used by Jones et al. [27] to calculate the ground vibration generated by a harmonic load moving on a surface railway track. Sheng et al. use this latter model to study the effects of changing the track/embankment structure with the track subjected to single and multiple moving harmonic and quasi-static loads [28]; combined with various vehicle models, they use it to predict the ground vibration due to vertical track irregularities from two ballasted tracks and one slab track [29], and to compare theoretical results with measured results at three different sites [30]. Lombaert et al. [31] validate a model comprising two rail beams on continuous layers representing railpad stiffness, sleeper mass and ballast stiffness, all resting on a horizontally layered half-space, with the train modelled as roughness-excited axle masses. The validation against measurements of soil dynamic response, track receptance and free field vibration produced by passing trains demonstrates the importance of the dynamic soil properties used in the model.

Several researchers have investigated track dynamics using FE models of beam tracks on non-rigid subgrades. Luo et al. [32] simulate the infinite soil under the track with a finite FE mesh with rigid boundary conditions; the soil mesh is made large enough that waves cannot return from the boundaries within the time considered. Sadeghi and Kohoutek [33] use a plane-strain FE model of the soil with viscous absorbing boundaries to determine the dynamic stiffness of the foundation for use in a beam track model. Esveld et al. [34] determine the response of a paved-in tramway with a discrete-element model of its different concrete-slab, asphalt and soil layers. Triantafyllidis and Prange [35,36] look at high-speed train energy loss associated with train–track interaction through a rail beam on rigid footings resting on a half-space represented using the boundary-element method (BEM). Auersch [37] uses a similar approach but with a layered soil, to compare predicted and measured dynamic axle loads and displacement magnitudes. Bode et al. [38] develop a time-domain formulation for the dynamic analysis of general three-dimensional FE models of structures resting on an elastic half-space. The formulation of soil behaviours requires only discretisation over the contact area as for BEM. They analyse the response of a railway track to a moving wheelset using the method, demonstrating the influence of "through-the-soil" coupling.

FE analysis of tracks and soil, often with BEM, has also frequently been used to predict ground vibration generated by surface railways. Girardi and Recchia [39] investigate the influence of sleeper type and ballast depth on ground response by means of a detailed FE track and vehicle model supported on a three-dimensional layered medium representing the ballast and subsoil, comparing results to under-track measurements. Takemiya [40] uses a "2.5-dimensional" FE track-embankment cross-section resting on a half-space represented by BEM to quantify the effect of a wave-impeding block (WIB) in the embankment under moving track loads. Takemiya and Goda [41] extend this to a layered half-space. A three-dimensional FEM–BEM treatment of a railway comprising two rail beams on rigid sleeper footings on a half-space is given in Mohammadi and Karabalis [42]. Madhus et al. [43] use a substructuring method to model the response of layered soil under an FE track model. Kaynia et al. [44] use a similar approach to model ground vibration from high-speed trains, finding good agreement with measurements for railways in southern Sweden.

Existing models for ground vibration from underground railways are summarised in the companion paper [1]. While some of the recent numerical models, particularly those based on a combined FE–BE approach, are able to model all the details of a specific underground railway system in three dimensions, the analytical models that do exist are often only two-dimensional, or do not consider the tunnel dynamics fully. Additionally, none treat detailed track models directly coupled to the tunnel, instead considering only general force inputs to the tunnel or soil. These omissions are in fact important, because in the problem frequency range of up to about 250 Hz [11], the wavelengths involved are typically of the order of the train axle spacing, the tunnel diameter and the distance of the tunnel from building foundations, so the interactions between these entities cannot be ignored. On the other hand, while beams on various continuous and discrete foundations, and quite detailed FEM–BEM models, have been used widely to investigate the dynamics of ballasted track and sometimes for the design of vibration-isolating track systems, the focus has been on surface railways and modelling viewpoints that conceptualise the ground as a half-space, with no provision for a tunnel and its interaction with the surrounding soil.

This paper aims to address the shortcomings of existing analytical models and provide an alternative to numerical approaches by creating a computationally efficient model that includes the major dynamic characteristics of the three-dimensional track, tunnel and soil system. It presents work originally developed in

the thesis [45]. Analytical techniques are utilised to minimise computational requirements. Beams on elastic layers are used to represent the various elements of a floating-slab track. After a brief overview of the tunnel model, a simple slab beam coupled to the tunnel is examined. Then another beam representing the rails, and masses representing a train's axles, are added to complete the track model. With roughness-displacement excitation between the axle masses and the rail beam, power-spectral densities (PSDs) and RMS vibration levels for the soil can be calculated, allowing the direct assessment of the effectiveness of the floating-slab track with varying support stiffness. In particular, this paper tests the hypothesis that floating-slab track is not always an effective means of vibration control.

2. Overview of the tunnel model

The derivation of the tunnel model is given in detail in Ref. [1]. The tunnel is conceptualised as an infinitely long thin cylindrical shell surrounded by soil of infinite radial extent. Fig. 1 shows the coordinate system and displacement and stress components for the cylindrical shell. These conventions are also used for the combined tunnel-in-soil model. The Flügge shell equations are used to model the tunnel and the wave equations for an elastic continuum are used to model the soil. The coupled problem is solved in the frequency domain by Fourier decomposition into ring modes circumferentially and a Fourier transform into the wavenumber domain longitudinally. The solution in the modal wavenumber-frequency domain takes the form

$$\begin{Bmatrix} \tilde{\mathbf{U}}_n \\ \mathbf{B} \end{Bmatrix} = \begin{bmatrix} [\mathbf{A}_E] & [\mathbf{T}_\infty]_{r=a} \\ [\mathbf{I}] & -[\mathbf{U}_\infty]_{r=a} \end{bmatrix}^{-1} \begin{Bmatrix} \tilde{\mathbf{P}}_n \\ \mathbf{0} \end{Bmatrix}, \tag{1}$$

where $\tilde{\mathbf{U}}_n = \{\tilde{U}_n\ \tilde{V}_n\ \tilde{W}_n\}^{\mathrm{T}}$ is the vector of displacements at the tunnel ($r = a$), $\mathbf{B} = \{B\ B_r\ B_z\}^{\mathrm{T}}$ is a vector of boundary-condition coefficients which arise from the solution for the elastic continuum, $\mathbf{0} = \{0\ 0\ 0\}^{\mathrm{T}}$, and $\tilde{\mathbf{P}}_n = \{\tilde{P}_{xn}\ \tilde{P}_{yn}\ \tilde{P}_{zn}\}^{\mathrm{T}}$ is the vector of stresses applied to the inside of the tunnel. The latter correspond to the *inside* components of q_x, q_y and q_z shown in Fig. 1(c). A unit normal point force acting on the tunnel invert at $\theta = 0$ has stress components $\tilde{P}_{xn} = \tilde{P}_{yn} = 0$ and $\tilde{P}_{zn} = 1/2\pi a$ for $n = 0$ and $\tilde{P}_{zn} = 1/\pi a$ for $n \geqslant 1$. The tilde on displacements and stresses indicates wavenumber-domain quantities, while n is the circumferential modenumber. The matrix $[\mathbf{A}_E]$ contains coefficients from the shell solution, $[\mathbf{I}]$ is a 3×3 identity matrix, and $[\mathbf{T}_\infty]_{r=a}$ and $[\mathbf{U}_\infty]_{r=a}$ contain coefficients that arise from the solutions for the continuum stresses and displacements, respectively, evaluated at the interface $r = a$. The elements of the shell and continuum matrices are functions of material properties as well as frequency ω, wavenumber ξ and modenumber n; the continuum ones are also a function of radius r. The tunnel displacements come directly from Eq. (1), but the soil displacements at a radius $r = R$ have to be calculated from

$$\tilde{\mathbf{U}}_n\big|_{r=R} = [\mathbf{U}_\infty]_{r=R} \cdot \mathbf{B} \tag{2}$$

using the coefficients $\mathbf{B}$ derived from Eq. (1).

The total wavenumber-domain displacements $\tilde{\mathbf{U}} = \{\tilde{U}\ \tilde{V}\ \tilde{W}\}^{\mathrm{T}}$ at a particular radius r and angular position θ are determined by using Fourier series to sum the modal components $\tilde{\mathbf{U}}_n$ calculated from Eqs. (1) or (2). Since

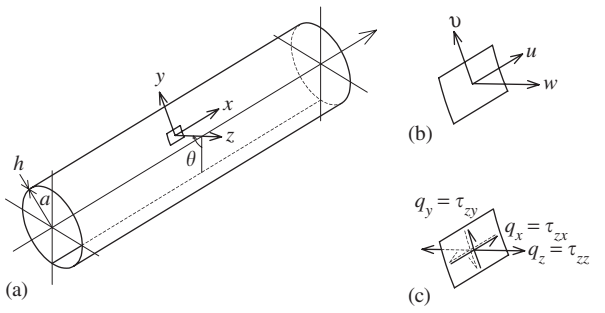

Fig. 1. The cylindrical shell used to model the tunnel, showing (a) the coordinate system for a typical element in the shell, (b) the corresponding displacement components and (c) the corresponding surface stress components. The length of the shell is taken as infinite.

Table 1
Parameter values used to model the tunnel surrounded by soil

Tunnel (cylindrical shell)	Soil (elastic continuum)
$E = 50 \times 10^9$ Pa	$E = 550 \times 10^6$ Pa
$\nu = 0.3$	$\nu = 0.44$
$\rho = 2500\,\mathrm{kg/m^3}$	$\rho = 2000\,\mathrm{kg/m^3}$
$c_1 = 5189\,\mathrm{m/s}$	$\lambda = 1.400 \times 10^9$ Pa
$c_2 = 2774\,\mathrm{m/s}$	$\mu = G = 191 \times 10^6$ Pa
$a = 3.0\,\mathrm{m}$	$K = 1.528 \times 10^9$ Pa
$h = 0.25\,\mathrm{m}$	$c_1 = 944\,\mathrm{m/s}$
Zero damping	$c_2 = 309\,\mathrm{m/s}$
	$\eta_G = 0.06$
	$\eta_K = 0$

the appropriate scaling is implicit in the load components $\tilde{\mathbf{P}}_n$ that are chosen, the result is

$$\left\{ \begin{array}{c} \tilde{U} \\ \tilde{V} \\ \tilde{W} \end{array} \right\}_r = \left\{ \begin{array}{c} \tilde{U}_0 \\ 0 \\ \tilde{W}_0 \end{array} \right\}_r + \sum_{n=1}^{\infty} \left\{ \begin{array}{c} \tilde{U}_n \cos n\theta \\ \tilde{V}_n \sin n\theta \\ \tilde{W}_n \cos n\theta \end{array} \right\}_r, \tag{3}$$

that is, the longitudinal and radial displacements $\tilde{U}$ and $\tilde{W}$ are Fourier cosine series, while the tangential displacement $\tilde{V}$ is a Fourier sine series. The displacements in the space domain can be obtained by an inverse spatial Fourier transform of Eq. (3).

Table 1 gives the values of the parameters used for the tunnel-in-soil model. E is Young's modulus, ν is Poisson's ratio, ρ is density, λ and μ are Lamé's constants with $\mu = G$, the shear modulus, and K is the bulk modulus. The wave speeds c_1 and c_2 are for pressure and shear waves, respectively. The tunnel has radius a and wall thickness h, and it is assumed that the concrete it is made of has negligible damping compared to the soil. Soil damping is characterised by the loss factors η_G associated with shear motion and η_K associated with volumetric expansion. It is assumed that all energy loss in the soil is through shear damping. With these parameter values, only modes up to $n = 10$ have to be considered in the summations of Eq. (3) to reach convergence with a normal point load.

3. A simple slab track

The simplest track model that can be combined with the tunnel is an infinitely long, continuous slab beam, as shown in Fig. 2. The approach used is similar to that employed by Ng [46] to join an infinite beam directly to an elastic half-space to model a surface railway. The slab beam and tunnel are joined along a single continuous line running longitudinally along the bottom of the tunnel invert. The coupling is achieved through the interaction force $G(x)$ which acts on the tunnel and its equal and opposite counterpart $-G(x)$ which acts on the beam. $F(x)$ is the external loading applied to the slab beam and is shown here as a point force.

3.1. Coupling equations for the simple slab beam and tunnel

Fig. 3 shows a general continuous distribution of time-harmonic force per unit length $Q(x)$ acting along a line such as the joining line on the slab beam or tunnel invert. The distributed force can be considered as a train of point loads represented by pulses of infinitesimal width $d(\chi)$ and magnitude $Q(\chi)$, so that the increment of the time-harmonic displacement response $Y(x)$ to one of these point loads is $\mathrm{d}Y(x) = H(x-\chi)Q(\chi)\,\mathrm{d}\chi$, where $H(x)$ is the frequency-response function (FRF) for $Y(x)$ to a point load acting at $x = 0$. Thus, the total displacement response is the sum of these increments over the whole length of the infinite joining line, giving

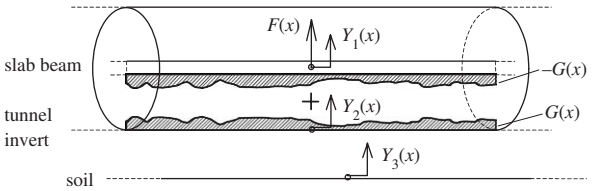

Fig. 2. Joining a simple slab beam of infinite length to the tunnel, showing the equal and opposite interaction forces acting on the beam and the tunnel.

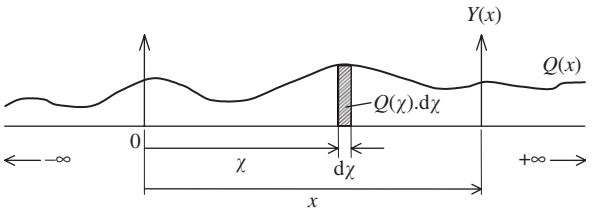

Fig. 3. General force distribution per unit length $Q(x)$ acting along a single line of joining. The displacement response $Y(x)$ is obtained by the convolution in space of the force increments $Q(\chi)\,\mathrm{d}\chi$ with the frequency-response function to a point load.

the integral

$$Y(x) = \int_{-\infty}^{\infty} H(x-\chi)Q(\chi)\,\mathrm{d}\chi, \tag{4}$$

which is a convolution (Duhamel) integral in space. This is equivalent to a Green's function formulation for the response, where $H(x-\chi)$ is Green's function. If the Fourier transform of both sides of Eq. (4) is taken using the first integral of the transform pair

$$\tilde{Y}(\xi) = \int_{-\infty}^{\infty} Y(x)\mathrm{e}^{-\mathrm{i}\xi x}\,\mathrm{d}x, \quad Y(x) = \frac{1}{2\pi}\int_{-\infty}^{\infty} \tilde{Y}(\xi)\mathrm{e}^{\mathrm{i}\xi x}\,\mathrm{d}\xi, \tag{5}$$

where ξ is angular wavenumber and the tilde indicates wavenumber-domain quantities, then Eq. (4) becomes

$$\tilde{Y}(\xi) = \tilde{H}(\xi)\tilde{Q}(\xi), \tag{6}$$

so that the convolution in space has been reduced to a simple multiplication in the wavenumber domain. Applying Eq. (6) to the coupled slab beam and tunnel invert in turn yields

$$\tilde{Y}_1 = \tilde{H}_{11}(-\tilde{G}+1), \quad \tilde{Y}_2 = \tilde{H}_{22}\tilde{G} \tag{7}$$

for the displacements $\tilde{Y}_1$ along the beam and $\tilde{Y}_2$ along the invert, when a unit point load acts on the slab at $x = 0$. The applied point load, additional to the interaction force, is equivalent to a force per unit length of $F = \delta(x)$, which gives $\tilde{F} = 1$ when transformed; hence the total ξ-domain force $(-\tilde{G}+1)$ acting on the slab beam. The functions $\tilde{H}_{11}$ and $\tilde{H}_{22}$ are the FRFs H_{11} (for the response of the free beam to a point load at $x = 0$) and H_{22} (for the response of the uncoupled tunnel invert to a point load at $x = 0$) in the wavenumber domain.

The slab beam can either be joined directly to the tunnel invert, or be supported on the invert via resilient slab bearings. For direct joining, the displacements of the slab and invert must be equal, so that in the wavenumber domain

$$\tilde{Y}_1 = \tilde{Y}_2. \tag{8}$$

Using Eq. (8) with Eq. (7) to eliminate $\tilde{G}$ gives

$$\tilde{Y}_1 = \tilde{Y}_2 = \frac{\tilde{H}_{11}\tilde{H}_{22}}{\tilde{H}_{11} + \tilde{H}_{22}} \tag{9}$$

for the displacements in the direct-joining case.

When the slab is joined to the invert via resilient slab bearings, the interaction force is determined by the extension of the bearings and their stiffness. If the bearings are modelled as a continuous resilient layer of stiffness k per unit length (like a Winkler foundation but without the rigid base), then the joining condition becomes

$$\tilde{G} = k(\tilde{Y}_1 - \tilde{Y}_2). \tag{10}$$

Using this new condition (10) with Eq. (7) yields

$$\tilde{Y}_1 = \frac{\tilde{H}_{11}(1 + k\tilde{H}_{22})}{1 + k\tilde{H}_{11} + k\tilde{H}_{22}}, \quad \tilde{Y}_2 = \frac{k\tilde{H}_{11}\tilde{H}_{22}}{1 + k\tilde{H}_{11} + k\tilde{H}_{22}} \tag{11}$$

for the displacements when the slab is joined to the tunnel via an elastic layer. Damping can be included to model a viscoelastic layer by using a complex stiffness value for k.

The response along a line in the soil parallel to the joining line (see Fig. 2) can be determined, once the displacement $\tilde{Y}_2$ is known, by using the second of Eq. (7) to find the interaction force $\tilde{G}$ which acts on the tunnel invert. The soil displacement is then

$$\tilde{Y}_3 = \tilde{H}_{32}\tilde{G} = \tilde{H}_{32}\frac{\tilde{Y}_2}{\tilde{H}_{22}} \tag{12}$$

for either joining method, where H_{32} is the FRF of a particular soil-displacement component Y_3 to a point force acting on the uncoupled tunnel invert at $x = 0$.

Any of the displacements found from Eqs. (9), (11) or (12) can be inverse Fourier-transformed from the wavenumber to the space domain by means of the second transform of the pair (5). With the unit point-load condition assumed, the physical displacements in the space domain represent the FRFs of the combined system for a point load acting at $x = 0$ on the slab beam.

It is worth noting that if the alternative definition of the Fourier transform pair is adopted, with the factor of $1/2\pi$ in the forward transform rather than the inverse one as in Eq. (5), then a factor of 2π appears on the right-hand side of the ξ-domain multiplication (6). This is then also true for Eq. (7), with the end result that every term containing a k in Eq. (11) is also multiplied by 2π. This extra complication is avoided by using definition (5).

3.2. Calculation of FRFs for simple coupling

The only quantities left to determine are the FRFs in the wavenumber domain for the tunnel-in-soil model and the slab beam before joining. The tunnel or soil displacements $\tilde{\mathbf{U}} = \{\tilde{U}\ \tilde{V}\ \tilde{W}\}^{\mathrm{T}}$ at a particular radius r and angular position θ which result from a spatial unit point load acting on the invert can be calculated using Eqs. (1)–(3) with the appropriate loading $\tilde{\mathbf{P}}_n$ as discussed in Section 2. The tunnel invert FRF $\tilde{H}_{22}$ is then $\tilde{W}$ for $r = a$ and $\theta = 0$, while the soil FRF $\tilde{H}_{32}$ can be whichever displacement component is of interest for any line in the soil defined by constant $r = R$ and $\theta = \beta$. Thus,

$$\tilde{H}_{22} = \tilde{W}\big|_{\substack{r=a\\ \theta=0}}, \quad \tilde{H}_{32} = \tilde{U},\ \tilde{V} \text{ or } \tilde{W}\big|_{\substack{r=R\\ \theta=\beta}}. \tag{13}$$

The FRF for the free beam can be determined from the equation of motion for its vertical displacement $y(x,t)$. For an Euler beam, this is (see Meirovitch [47])

$$m\frac{\partial^2 y}{\partial t^2} + EI\frac{\partial^4 y}{\partial x^4} = f(x,t), \tag{14}$$

where m is the beam's mass per unit length, EI is its bending stiffness (E Young's modulus and I the second moment of area), and $f(x,t)$ is the applied force per unit length. Substituting a harmonic solution $y = \tilde{Y}e^{i(\omega t + \xi x)}$

with a force $f = \tilde{F}e^{i(\omega t+\xi x)}$ of the same form yields

$$\tilde{H}_{YF} = \tilde{Y}|_{\tilde{F}=1} = \frac{1}{EI\xi^4 - m\omega^2}. \tag{15}$$

Using harmonic solutions in this way is equivalent to taking the Fourier transform of Eq. (14) twice, once each for time to frequency and space to wavenumber domains. The force $\tilde{F} = 1$ represents a unit spatial point load acting at $x = 0$ as discussed above. Thus, the free-beam FRF $\tilde{H}_{11}$ is simply

$$\tilde{H}_{11} = \tilde{H}_{YF}. \tag{16}$$

3.3. Results for the tunnel with a simple slab beam

As mentioned earlier, the slab beam can be joined either directly to the tunnel invert or via slab bearings, represented by springs. Either case can be compared to the Winkler beam model often used for track design, as shown in Fig. 4. To allow comparison of results, the Winkler frequency response $Y(x,\omega)$ must be determined. This is easily obtained by applying Eq. (14) to an infinite beam on an elastic foundation, giving

$$Y(x,\omega) = \frac{1}{4\alpha^3 EI}(e^{\alpha|x|} + ie^{i\alpha|x|}), \quad \text{with } \alpha^4 = \frac{m\omega^2 - k_W}{EI}, \tag{17}$$

where k_W is the stiffness per unit length of the elastic foundation. The root α used is the second-quadrant one, so that both α and $i\alpha$ have negative real parts and the two exponentials in Eq. (17) decay as $|x| \to \infty$. To make the Winkler beam "equivalent" to the slab beam on the tunnel, its static displacement at $x = 0$ is equated to the numerical value for the static displacement of the directly joined slab beam, resulting in k_W being the effective Winkler stiffness k_{eff} of the tunnel invert, as depicted in Figs. 4(a) and (b). If the slab is then supported on bearings of stiffness k per unit length, Fig. 4(c), the equivalent Winkler beam has the additional stiffness added in series, Fig. 4(d), giving $k_W = 1/(1/k_{\text{eff}} + 1/k)$. The Winkler beam has a resonance at $\omega_n = \sqrt{k_W/m}$ as can be seen from Eq. (17), so k can be selected to give specific Winkler "natural frequencies". Classic vibration-isolation theory using a mass on a spring predicts that isolation should be achieved at frequencies greater than $\sqrt{2}\omega_n$; this assumption can now be tested.

The displacements of the slab-plus-tunnel model were calculated from Eqs. (9), (11) or (12) as required. The inverse Fourier transforms into the space domain were carried out numerically using an inverse fast Fourier transform (FFT). The values of the parameters for the slab beam and its support stiffness are given in Table 2. The tunnel FRFs were calculated as described in the companion paper [1] and outlined in Section 2, using the parameters in Table 1. In conjunction with the slab properties, these determine the effective stiffness k_{eff} of the tunnel invert for use with the equivalent Winkler beam. Once the effective stiffness is calculated, the

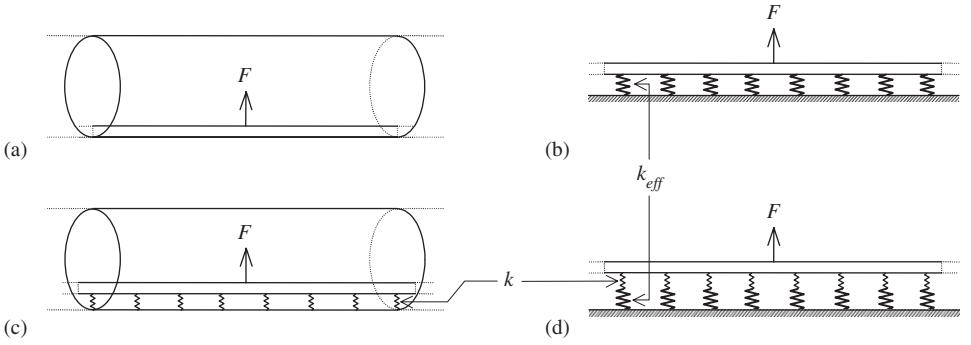

Fig. 4. A simple slab beam joined (a) directly to the tunnel invert and compared to (b) an "equivalent" Winkler beam on the effective stiffness of the tunnel invert. The slab beam (c) with resilient bearings between it and the tunnel can then be compared to (d) the "equivalent" Winkler beam with the extra foundation stiffness of the bearings added in series.

Table 2
The simple slab beam's properties, the effective stiffness of the tunnel invert described by the parameters of Table 1, and three resulting slab-support stiffnesses

Simple slab beam
$EI = 1430 \times 10^6\,\mathrm{Pa\,m^4}$
$m = 3500\,\mathrm{kg/m}$
$k_{\mathrm{eff}} = 821.2 \times 10^6\,\mathrm{N/m^2}$
$\eta_{\mathrm{eff}} = 0.0643$
$k = 1262 \times 10^6\,\mathrm{N/m^2}$ when $f_n = 60\,\mathrm{Hz}$
$k = 424.4 \times 10^6\,\mathrm{N/m^2}$ when $f_n = 45\,\mathrm{Hz}$
$k = 146.6 \times 10^6\,\mathrm{N/m^2}$ when $f_n = 30\,\mathrm{Hz}$
$\eta_k = 0.5$

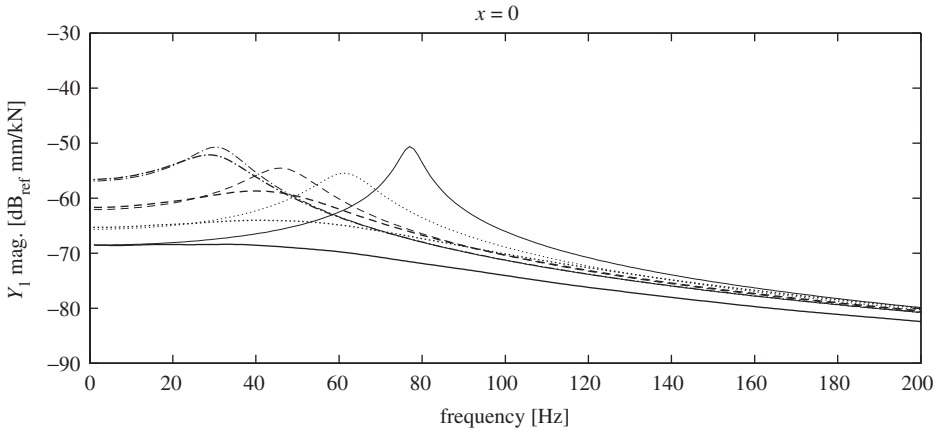

Fig. 5. Vertical driving-point displacement response of a simple slab beam on the tunnel (normal weight lines) compared to the "equivalent" Winkler beam (lighter weight lines) for direct joining —— and support stiffnesses for Winkler "natural frequencies" of 60 Hz ·····, 45 Hz - - - - - and 30 Hz - · - · -.

slab-support stiffnesses can be determined for various Winkler natural frequencies. Three stiffnesses are given in Table 2 for increasingly softer support.

Damping in the springs is hysteretic, described by a constant loss factor such that complex stiffnesses $k(1+i\eta)$ are substituted for real stiffnesses k. The calculated loss factor η_{eff} is very close to the shear loss factor given in Table 1 for the soil. The loss factor of $\eta_k = 0.5$ for the slab-support stiffness is relatively high but not unreasonable for rubber with high damping (see data in Ref. [48] for instance). Its value is also influenced by the numerical considerations arising from the Nyquist criterion for the inverse FFT. For frequencies up to 200 Hz, a spacing of $\Delta x = 0.5\,\mathrm{m}$ was found sufficient to capture all the wavenumber information of the slab-plus-tunnel model, and with $N = 2048$ points and the given loss factor, the response of the slab beam decayed sufficiently at the sample ends in both ξ- and x-domains for the FFT to be considered an accurate representation of the Fourier transform. The symmetry of the responses in both domains means that all ξ-domain calculations could be done for the 1025 points of the sample with $\xi \geqslant 0$, and the portion for $\xi < 0$ created by a suitable reflection just prior to the inverse FFT.

Fig. 5 shows the driving-point response of the slab beam for the various slab-support stiffnesses, compared to that of an "equivalent" Winkler beam in each case. The directly joined slab shows a flat response, while the corresponding Winkler response shows a clear resonance just below 80 Hz. The energy of the slab beam is radiated into the soil quite effectively when the slab is closely coupled to the tunnel, whereas this radiation damping effect is not accounted for in the loss factors of the elastic foundation of the Winkler beam. As the

slab-support stiffness is reduced, the slab response gets closer to the Winkler response, until the two almost coincide for $f_n = 30$ Hz. With lower values of k, the slab beam is less strongly coupled to the tunnel, or in other words, the tunnel becomes more like a rigid foundation (compare the values of k with the value of k_{eff} in Table 2). Although the 30 Hz frequency is relatively high compared to some design natural frequencies, it does represent "soft" bearings for the given tunnel properties, as can be seen from the coincidence with its equivalent Winkler model. The 30 Hz case is therefore representative of actual floating-slab tracks as designed.

At this point it might be assumed that for realistic, soft bearings, the Winkler theory adequately describes the behaviour of a floating slab. However, a glance at Fig. 6, which gives responses at 20 m from the load, shows that this is not the case. The slab beam supported by the tunnel has significant response at low frequencies no matter what value k has, while the equivalent Winkler beams do not show much response below the Winkler natural frequencies, above which travelling waves occur and propagate energy along the beam. This illustrates how the tunnel can transmit energy to the coupled slab beam even when there are no travelling waves in the slab itself.

Even if the Winkler theory were adequate for describing the slab beam, it cannot predict the response of the tunnel invert and the soil surrounding the tunnel. Fig. 7 shows the vertical response of the invert directly beneath the load applied to the slab at $x = 0$. Small circles mark the $\sqrt{2}f_n$ frequencies above which, according

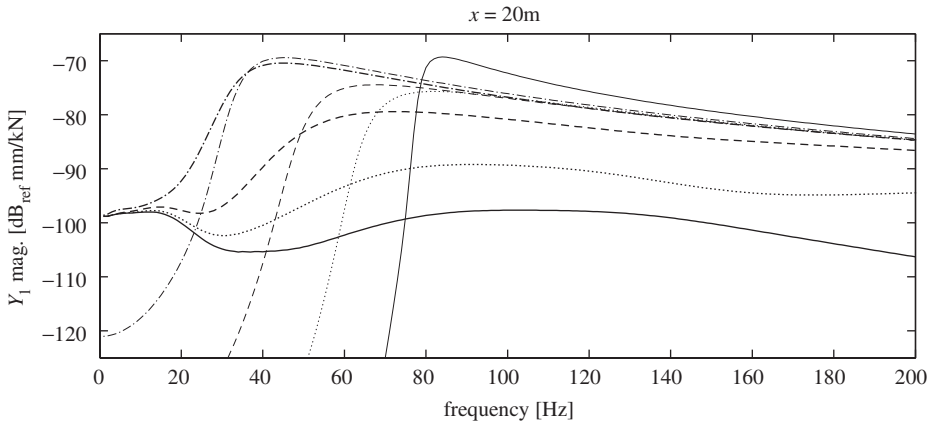

Fig. 6. Vertical displacement response of the simple slab beam 20 m from the load (normal weight lines), compared to the "equivalent" Winkler beam (lighter weight lines) for direct joining —— and 60 Hz ·····, 45 Hz - - - - - - and 30 Hz - · - · - · support stiffnesses.

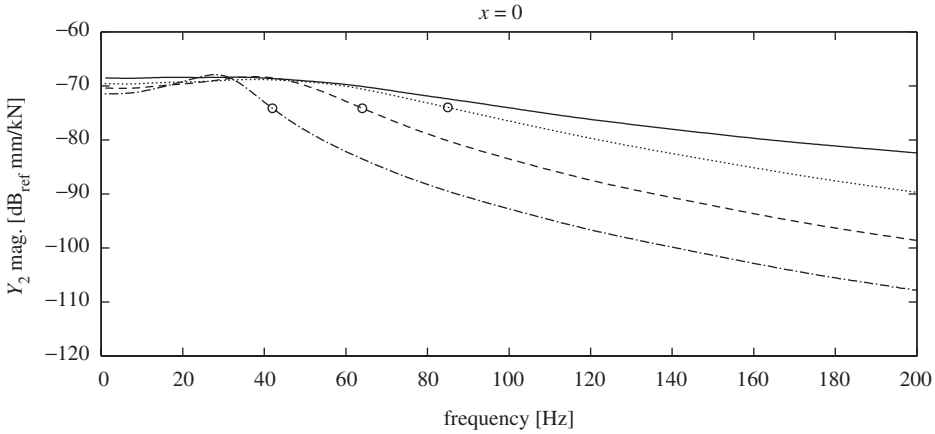

Fig. 7. Vertical displacement response of the tunnel invert directly under the load on the slab beam for direct joining —— and 60 Hz ····· , 45 Hz - - - - - - and 30 Hz· · · · · · support stiffnesses, with circles marking the $\sqrt{2}f_n$ points.

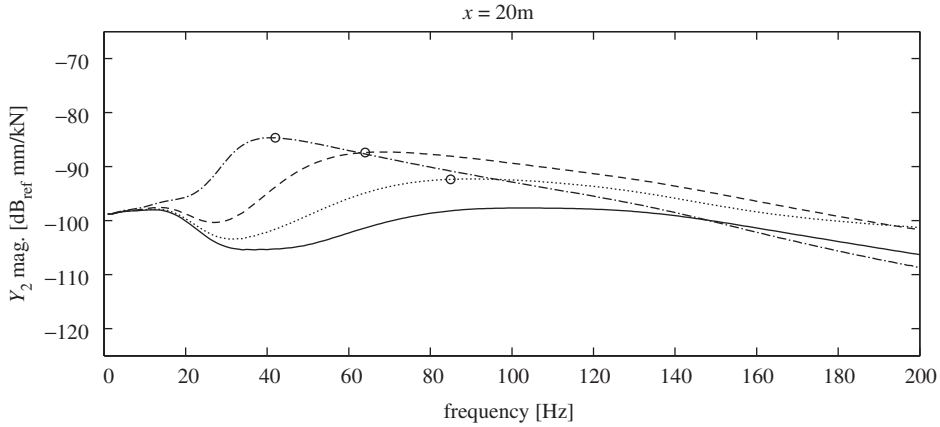

Fig. 8. Vertical displacement response of the tunnel invert 20 m along the tunnel from the load applied to the slab beam, for direct joining —— and 60 Hz ·····, 45 Hz - - - - - and 30 Hz - · - · - · - support stiffnesses, with circles marking the $\sqrt{2}f_n$ points.

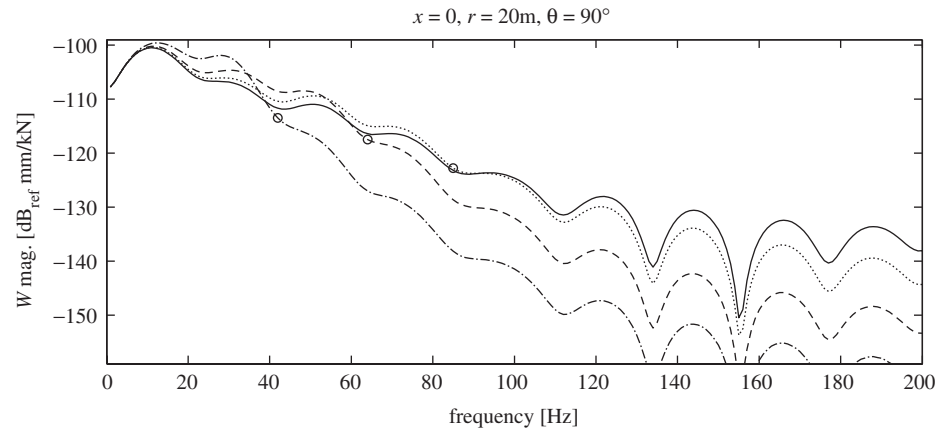

Fig. 9. Horizontal soil displacement response 20 m horizontally out into the soil opposite the load on the slab for direct joining —— and 60 Hz ·····, 45 Hz - - - - - and 30 Hz ····-·-·-····support stiffnesses, with circles marking the $\sqrt{2}f_n$ points.

to simple theory, vibration isolation is supposed to occur. It can be seen in this case that the responses for a slab on bearings drop below the response of the directly joined slab well before these cut-off points, so simple vibration-isolation theory holds so far. However, the response 20 m along the tunnel invert, shown in Fig. 8, is actually made *higher* by the insertion of rubber between the slab and the invert, with only the softest bearings ($f_n = 30$ Hz) eventually giving a lower response at about 145 Hz. The higher responses are to be expected since the bearings decouple the slab from the tunnel and hence allow energy to propagate further along the beam before being transmitted to the invert. This is not necessarily a problem: it could indeed be beneficial if it means that vibrational energy is confined to the slab beam and the tunnel and is not radiated into the soil.

The most important measure of the isolation effectiveness of a track is the vibration level in the soil. Soil responses will be given here for the horizontal plane $\theta = 90^\circ$, so that the displacement components W and V coincide with the horizontal and vertical directions. Fig. 9 shows the horizontal soil displacement at a radius of 20 m horizontally out into the soil, opposite the load on the slab. The responses exhibit the peaks and troughs of a pressure-wave interference pattern arising from energy propagating from different parts of the tunnel into the soil. This is as was also observed and discussed for the uncoupled tunnel in Ref. [1]. At this position in the soil, increasingly softer slab support results in reduction starting at frequencies near the $\sqrt{2}f_n$ points, again marked with circles, obeying simple vibration-isolation theory just as the tunnel invert did directly under the

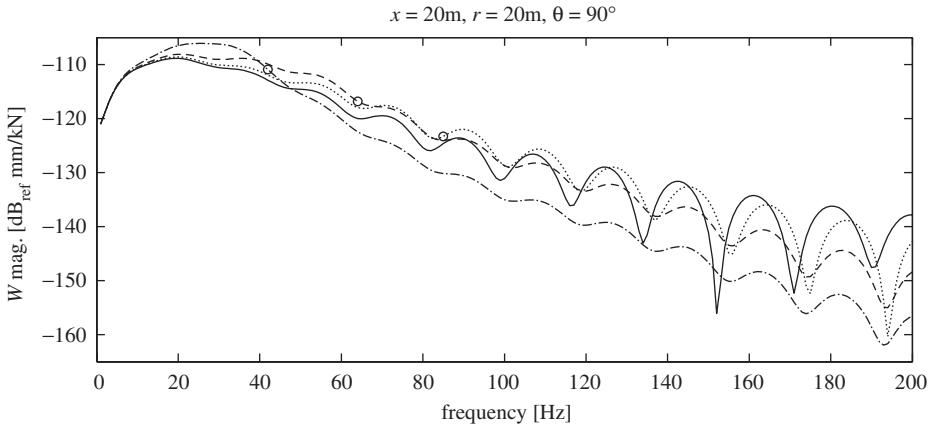

Fig. 10. Horizontal soil displacement response 20 m horizontally out into the soil and 20 m longitudinally parallel to the tunnel from the slab load, for direct joining —— and 60 Hz ·····, 45 Hz - - - - - and 30 Hz - · - · - support stiffnesses, with circles marking the $\sqrt{2}f_n$ points.

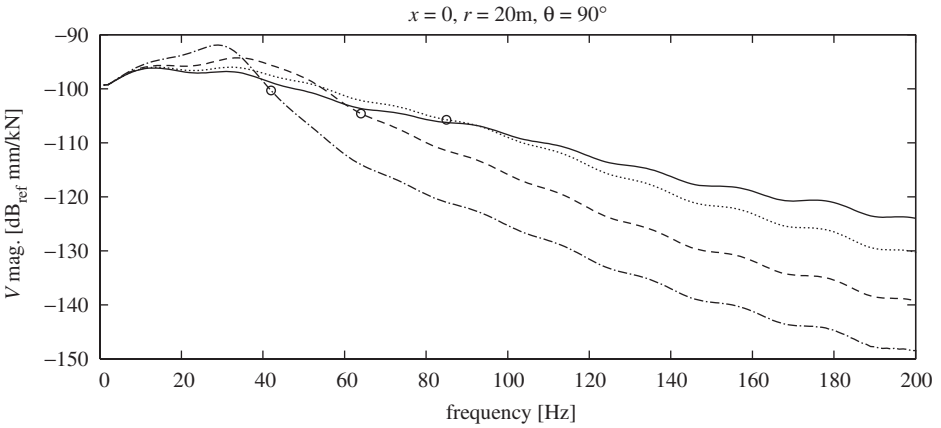

Fig. 11. Vertical soil displacement response 20 m horizontally out into the soil from the load, for direct joining —— and 60 Hz ·····, 45 Hz - - - - - - and 30 Hz ···· - ···· - support stiffnesses, with circles marking the $\sqrt{2}f_n$ points.

slab load. Fig. 10 shows similar behaviour for the horizontal response at $x = 20$ m, although now isolation is delayed somewhat (the "isolated" responses cross the directly joined response at higher frequencies than before), because at frequencies near the resonance the slab on bearings is propagating energy further along the tunnel before it enters the soil.

The vertical soil response at 20 m radius opposite the load, Fig. 11, also shows classic vibration isolation, this time very clearly because the pressure-wave effects are subdued. But as the observation point is shifted longitudinally, this behaviour changes. Fig. 12 shows that, at $x = 20$ m, the insertion of the stiffer rubber bearings ($f_n = 60$ and 45 Hz) has almost no effect on the vertical soil displacement, while for the softest bearings ($f_n = 30$ Hz) only a modest, roughly constant reduction of 5–10 dB is achieved, rather than an ever-increasing reduction with frequency as exhibited in Fig. 11 (and expected from simple isolation theory). At $x = 40$ m, Fig. 13, adding any slab bearings at all increases the vertical displacement for all frequencies between 40 and 200 Hz. This can again be explained by the transmission of energy along the slab on bearings, giving higher response at the portion of the tunnel nearest the observation point. The longitudinal soil response at $x = 20$ m, given in Fig. 14, is very similar to the horizontal response given in Fig. 10, showing the

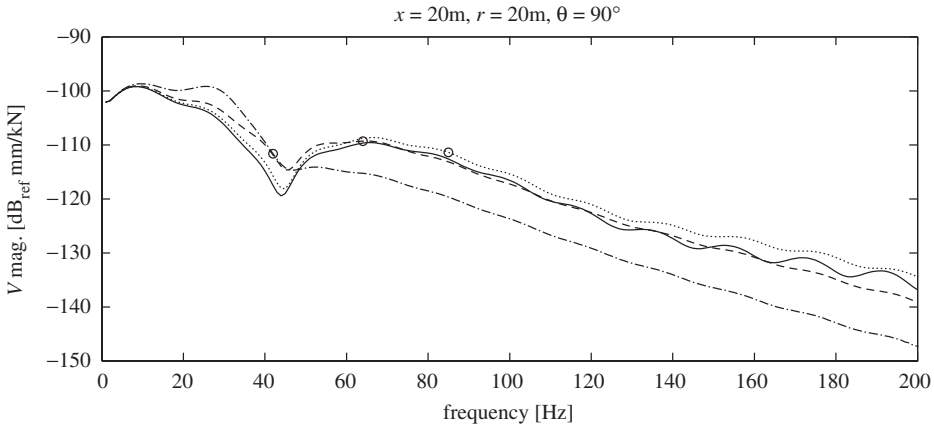

Fig. 12. Vertical soil displacement response 20 m horizontally out into the soil and 20 m longitudinally parallel to the tunnel from the slab load, for direct joining —— and 60 Hz ·····, 45 Hz - - - - and 30 Hz - · - · - support stiffnesses, with circles marking the $\sqrt{2}f_n$ points.

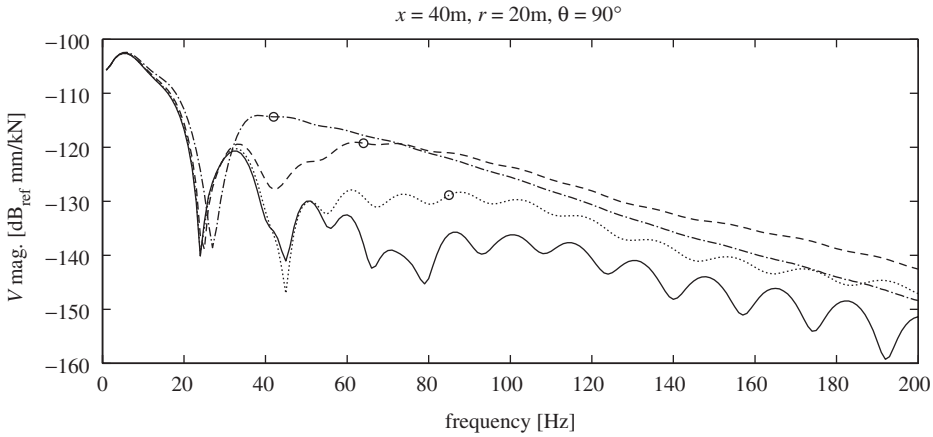

Fig. 13. Vertical soil displacement response 20 m horizontally out into the soil and 40 m longitudinally parallel to the tunnel from the slab load, for direct joining —— and 60 Hz·····, 45 Hz - - - - - - and 30 Hz ···· - - - support stiffnesses, with circles marking the $\sqrt{2}f_n$ points.

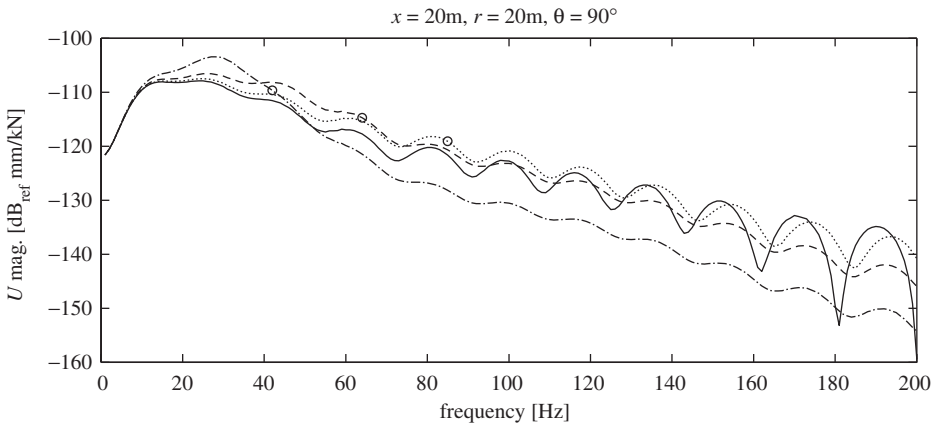

Fig. 14. Longitudinal soil displacement 20 m horizontally out into the soil and 20 m longitudinally parallel to the tunnel from the slab load, for direct joining —— and 60 Hz·····, 45 Hz - - - - - - and 30 Hz···· - - - support stiffnesses, with circles marking the $\sqrt{2}f_n$ points.

same type of delayed isolation, for the same reason (the longitudinal displacement at $x = 0$ is zero because it is an odd function of x).

The results discussed above have considered the responses to a single load acting on the slab beam. In reality a train provides a series of simultaneous inputs to the track. This means that the total response at an observation point in the soil will be some kind of sum of the responses for the various loads applied at different points along the track. Taking the vertical displacement component as an example, this would be the sum of the responses (among others) represented by Figs. 11–13. The magnitudes of these separate responses are all of the same order (near −120 dB), but with slab bearings sometimes reducing response and sometimes increasing it. Whether floating the slab gives a beneficial reduction in soil vibration depends on how these various responses add up.

The simple slab beam model can be extended by including beam torsion and considering two parallel lines for coupling the slab to the tunnel. This extended model is treated in the thesis [45]. Here, however, the immediate interest is in including the effects of the rails and multiple axle inputs on them in order to assess the true effectiveness of floating-slab track.

4. A full track comprising a simple slab, rail beam and axle masses

As well as the effects of the track slab, a track model should take the dynamics of the rail and the train interacting with it into account. An improved track model is shown in Fig. 15. It consists of a simple slab beam supporting a rail beam (representing the two rails together) with masses placed at intervals to represent the axle–wheel assemblies of a train. The slab and rail beams are infinitely long. The axle masses are a first-approximation train model which only considers the unsprung mass of the train, assuming that the primary suspension isolates the rest of each vehicle in the train. Real train vehicles have pairs of axles attached to bogies, which also contribute to the low-frequency interaction with the rail (below and around the primary natural frequency of suspensions, that is, below about 20 Hz). However, the important frequencies for ground-borne vibration from underground railways are well above this region (for example, Heckl et al. [49] give data which shows that the peak levels in transmitted ground vibration occur between about 40 and 80 Hz). Therefore, the bogie dynamics are not significant for the current problem. Also neglected is a Hertzian contact spring between each wheel and the rail, because this only plays a role at frequencies higher than those of interest (for example, Clark et al. [50] conclude that the Hertzian contact does not have a significant effect on rail response below 750 Hz). Although slab tracks with direct fasteners or embedded rails can have very high stiffnesses of the same order as the Hertzian contact, this would nevertheless still be a factor influencing track behaviour at relatively high frequencies. At the low frequencies that are important in ground vibration, these high stiffnesses would present an effectively rigid connection to the slab, and would have negligible effect as stiffnesses per se compared to resilient slab bearings. In any case, it would be fairly straightforward to include

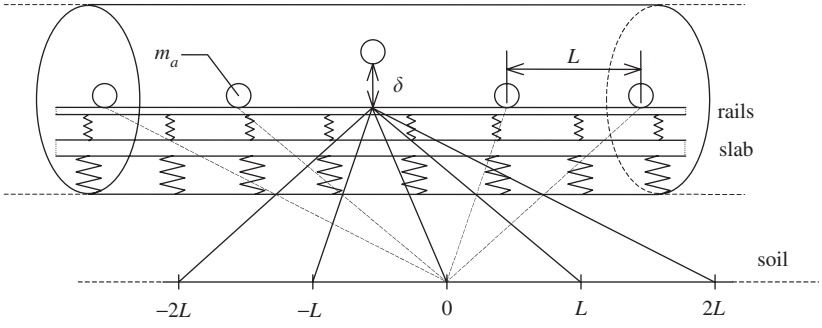

Fig. 15. Full-track model supported on the tunnel invert, with masses added to represent axles of a train. The centre mass is excited by a roughness displacement input δ. The tunnel's infinite length means the responses at one point in the soil to each axle input (paths with dashed lines) are equivalent to the line of separate responses to the single input shown (paths with solid lines) for an infinite number of masses at regular spacing.

Hertzian contact in the model if desired, by including extra terms in the dynamic-stiffness expressions for the axle masses in addition to the simple inertia terms that will be sufficient for the current track model.

The aim is to find the response at a single representative point in the soil when there is a series of input loads along the rails due to a train running on the track. For just one input load, the infinite length of the tunnel means that the load and the observation point can be *shifted* longitudinally while maintaining their separation, and the response at the observation point will not change. In other words, the response in the soil at $x = 0$ to a load on the rail at $x = L$ is always identical to the response at $x = -L$ to the same load at $x = 0$. (For tangential and radial soil-response components, which are even functions of x, it is also identical to the response at $x = L$ to the load at $x = 0$, so that only the magnitude of the separation matters.) Hence, the problem of finding the set of FRFs for the soil response at $x = 0$ to a set of loads at various positions on the rail can be recast into the problem of finding the FRFs for the soil at those various longitudinal positions to a single load at $x = 0$. The shifting principle for a tunnel and track model with axle masses is depicted in Fig. 15. Note that in this case it only works for an infinite number of axle masses at regular spacing, so that the overall model remains infinite and the longitudinal symmetry is maintained with any amount of shifting. Nevertheless, when the shifting principle is invoked so that only an input at the middle axle ($x = 0$) is used, a finite number of axles is sufficient if there are enough of them that the responses of the model do not change with more axles added at the ends, that is, a convergence has been reached.

The total soil response due to all the axle loads acting simultaneously can be calculated by adding up all the FRFs for an input at $x = 0$, after scaling and phasing each one appropriately. If the train is infinitely long and the inputs random, the sum represents the response anywhere along the soil line and thus condenses the three-dimensional problem represented by the individual FRFs to a two-dimensional problem of the vibration level at a particular point in the cross-section of the tunnel and soil.

4.1. Joining a rail beam to the slab-plus-tunnel model

The easiest way to construct the basic track model is to add a rail beam to the combined slab-plus-tunnel model of Section 3, using the principle of convolution in space. The coupling Eq. (11) are therefore applied to the rail beam and slab-plus-tunnel as the two entities to be joined. To avoid confusion with the numerals already used in Section 3 to denote the lines along the slab (1), the tunnel invert (2) and the soil (3), the line along the rail beam will be denoted by 0 (zero). Thus, the vertical rail and slab responses $\tilde{Y}_{0a}$ and $\tilde{Y}_{1a}$ of the new combined system to a vertical unit spatial point load acting on the rail beam at $x = 0$ are

$$\tilde{Y}_{0a} = \frac{\tilde{H}_{00a}(1 + k_r\tilde{H}_{11a})}{1 + k_r\tilde{H}_{00a} + k_r\tilde{H}_{11a}}, \quad \tilde{Y}_{1a} = \frac{k_r\tilde{H}_{00a}\tilde{H}_{11a}}{1 + k_r\tilde{H}_{00a} + k_r\tilde{H}_{11a}}, \tag{18}$$

where $\tilde{H}_{00a}$ is the ξ-domain FRF for the unjoined rail beam, $\tilde{H}_{11a}$ is the ξ-domain FRF of the slab beam to a load on the slab before the rail is added, and k_r is the stiffness per unit length of the resilient layer between the rail and slab beams. In the same way as Eq. (12), responses along lines not involved in the joining can be determined by means of the coupling interaction force. In this case the interaction force acts on the slab beam and is given by the response of the slab in the new combined model divided by its pre-rail-beam FRF, that is, $\tilde{Y}_{1a}/\tilde{H}_{11a}$. Hence, the responses $\tilde{Y}_{2a}$ along the tunnel invert and $\tilde{Y}_{3a}$ in the soil are

$$\tilde{Y}_{2a} = \tilde{H}_{21a}\frac{\tilde{Y}_{1a}}{\tilde{H}_{11a}}, \quad \tilde{Y}_{3a} = \tilde{H}_{31a}\frac{\tilde{Y}_{1a}}{\tilde{H}_{11a}}, \tag{19}$$

where $\tilde{H}_{21a}$ and $\tilde{H}_{31a}$ are the ξ-domain FRFs of the tunnel invert and the soil to a load on the pre-rail-beam slab. The physical displacement functions in the x-domain can be obtained by the inverse Fourier transform of results (18) and (19) according to Eq. (5).

The FRFs of the slab, tunnel and soil displacements which appear in Eqs. (18) and (19) are just the displacements determined by Eqs. (11) and (12) for the slab-plus-tunnel model. The FRF for the rail beam is that given by Eq. (15) for a free beam, but now with the properties of the two rails instead of the slab. Thus,

$$\tilde{H}_{00a} = \tilde{H}_{YF}, \quad \tilde{H}_{11a} = \tilde{Y}_1, \quad H_{21a} = \tilde{Y}_2, \quad \tilde{H}_{31a} = \tilde{Y}_3. \tag{20}$$

4.2. Adding axle masses to the rail beam

Adding axle masses to the model constructed so far is most simply done in the space domain. Since the axles interact with the rail, the coupled rail's x-domain FRF $H_0(x)$ is required. This can be obtained by the inverse Fourier transform of the ξ-domain result from Eq. (18), that is,

$$H_0(x) = \frac{1}{2\pi}\int_{-\infty}^{\infty} \tilde{Y}_{0a}(\xi)\mathrm{e}^{\mathrm{i}\xi x}\,\mathrm{d}\xi, \tag{21}$$

which represents the FRF of the rail to a point load acting at $x = 0$ on the rail, at a particular frequency ω. To find the final response in the soil, the soil's x-domain FRF $H_3(x)$ to the same load on the rail is required. This latter FRF is obtained in the same way as $H_0(x)$, but from result (19), so that

$$H_3(x) = \frac{1}{2\pi}\int_{-\infty}^{\infty} \tilde{Y}_{3a}(\xi)\mathrm{e}^{\mathrm{i}\xi x}\,\mathrm{d}\xi, \tag{22}$$

where $\tilde{Y}_{3a}(\xi)$ can be the u, v, or w component of soil displacement.

As the first step in the addition of axle masses, the rail responses at the positions where the masses are to be added must be formed into an FRF matrix $[\mathbf{H}_0]$, which satisfies

$$\mathbf{Y}_0 = [\mathbf{H}_0]\mathbf{F}_0, \tag{23}$$

where $\mathbf{Y}_0$ is the vector of rail displacements at the stations where masses will be added, and $\mathbf{F}_0$ is the vector of forces acting at those positions on the rail (once masses are added, these will be the interaction forces between the masses and the rail). Keeping this in mind, it is interesting to note that Eq. (23) is exactly analogous to the convolutions in space presented earlier. While convolution was used to find the function of responses along a line to a *continuous* interaction force acting along that line, the matrix multiplication here is used to find the *vector* of responses along a line to a set of *discrete* interaction forces acting on the line. The elements of the matrix $[\mathbf{H}_0]$ are determined by the rail-displacement FRF $H_0(x)$ of Eq. (21) as described below.

The case of adding only five masses will be considered here as an example of the general approach. It can easily be extended to more added masses to give the convergence necessary to model an infinitely long train. The infinite length and the symmetry of the track and tunnel mean that a given rail FRF is only dependent on the magnitude of the separation between the displacement and load involved, as discussed earlier in the context of soil displacements. If a regular axle spacing of L is used, the rail FRF matrix is

$$[\mathbf{H}_0] = \begin{bmatrix} H_0(0) & H_0(L) & H_0(2L) & H_0(3L) & H_0(4L) \\ H_0(L) & H_0(0) & H_0(L) & H_0(2L) & H_0(3L) \\ H_0(2L) & H_0(L) & H_0(0) & H_0(L) & H_0(2L) \\ H_0(3L) & H_0(2L) & H_0(L) & H_0(0) & H_0(L) \\ H_0(4L) & H_0(3L) & H_0(2L) & H_0(L) & H_0(0) \end{bmatrix}. \tag{24}$$

To facilitate the process of adding axles, the FRF matrix $[\mathbf{H}_0]$ of Eq. (24) should be inverted, allowing the dynamic-stiffness expression

$$\mathbf{F}_0 = [\mathbf{H}_0]^{-1}\mathbf{Y}_0 = [\mathbf{K}_0]\mathbf{Y}_0 \tag{25}$$

to be written. Axles are then added to the model as concentrated masses m_a by adding inertia terms of the form $-m_a\omega^2 Y$, where Y is the displacement at the axle's station, to the appropriate diagonal elements of the dynamic-stiffness matrix $[\mathbf{K}_0]$, leaving the centre station free. An axle mass is added to this centre station via a

roughness displacement $\delta = \Delta e^{i\omega t}$, as shown in Fig. 15. The overall matrix equation then becomes

$$\begin{bmatrix} k_{11}-m_a\omega^2 & k_{12} & k_{13} & k_{14} & k_{15} & 0 \\ k_{21} & k_{22}-m_a\omega^2 & k_{23} & k_{24} & k_{25} & 0 \\ k_{31} & k_{32} & k_{33} & k_{34} & k_{35} & -m_a\omega^2 \\ k_{41} & k_{42} & k_{43} & k_{44}-m_a\omega^2 & k_{45} & 0 \\ k_{51} & k_{52} & k_{53} & k_{54} & k_{55}-m_a\omega^2 & 0 \\ 0 & 0 & -1 & 0 & 0 & 1 \end{bmatrix} \begin{Bmatrix} Y_1 \\ Y_2 \\ Y_3 \\ Y_4 \\ Y_5 \\ Y_a \end{Bmatrix} = \begin{Bmatrix} 0 \\ 0 \\ 0 \\ 0 \\ 0 \\ \Delta \end{Bmatrix}, \tag{26}$$

where the k_{ij} are the elements of $[\mathbf{K}_0]$. Eq. (26) is of order one greater than the original dynamic-stiffness matrix because of the extra displacement component Y_a introduced by the independent axle mass at the centre.

After the displacements of the rail at the axle masses have been calculated from Eq. (26), the corresponding interaction forces $\mathbf{F}_0$ acting on the rail at the mass stations can be determined by substituting the vector of displacements $\mathbf{Y}_0 = \{Y_1\ Y_2\ Y_3\ Y_4\ Y_5\}^{\mathrm{T}}$ (that is, omitting Y_a) back into Eq. (25). Knowing the interaction forces which act on the rail, the soil displacements $\mathbf{Y}_3$ can be found from the FRF function $H_3(x)$ given by Eq. (22). In matrix form this can be expressed as

$$\mathbf{Y}_3 = [\mathbf{H}_3]\mathbf{F}_0, \tag{27}$$

where $[\mathbf{H}_3]$ is the FRF matrix for the soil line to input forces acting on the rail (with no axle masses added). For the tangential and radial components of soil displacement, V and W, $[\mathbf{H}_3]$ is of the same form as $[\mathbf{H}_0]$ given by Eq. (24), but with $H_3(x)$ replacing $H_0(x)$. This is because these components are even functions of x for a vertical load applied at $x = 0$, just like the vertical displacements of the rail. However, the longitudinal component U is an odd function of x for such a load, so that the sign of the longitudinal separation between a given load and displacement is important. The soil FRF matrix for longitudinal displacement is therefore given by

$$[\mathbf{H}_3^u] = \begin{bmatrix} H_3^u(0) & -H_3^u(L) & -H_3^u(2L) & -H_3^u(3L) & -H_3^u(4L) \\ H_3^u(L) & H_3^u(0) & -H_3^u(L) & -H_3^u(2L) & -H_3^u(3L) \\ H_3^u(2L) & H_3^u(L) & H_3^u(0) & -H_3^u(L) & -H_3^u(2L) \\ H_3^u(3L) & H_3^u(2L) & H_3^u(L) & H_3^u(0) & -H_3^u(L) \\ H_3^u(4L) & H_3^u(3L) & H_3^u(2L) & H_3^u(L) & H_3^u(0) \end{bmatrix} \tag{28}$$

for regular axle spacing of L.

4.3. Random process theory applied to the full-track model

The roughness and other irregularities of real rail and wheel surface profiles will be randomly distributed, so the roughness-displacement inputs at the wheels of a train travelling on the track will be random processes. The calculation of the resultant soil responses therefore requires the use of the theory of random vibration, which is dealt with by Newland [51], whose approach will be used here.

A random process is stationary if its mean, mean square and standard deviation are independent of time. Consider a system with N stationary random inputs x_j (such as the axle inputs provided by a train) and one (stationary random) output y (such as the displacement response of a particular point in the soil). The power-spectral density (PSD), or spectrum, $S_y(\omega)$ of the output process y is then given by

$$S_y(\omega) = \sum_{p=1}^{N}\sum_{q=1}^{N} H_p^*(\omega)H_q(\omega)S_{x_p x_q}(\omega), \tag{29}$$

where $H_p(\omega)$ and $H_q(\omega)$ are the FRFs of y to the inputs x_p and x_q, respectively (with star denoting the complex conjugate), and $S_{x_p x_q}(\omega)$ is the cross-spectral density, or cross-spectrum, between the two inputs. If two input processes have the same statistical properties, that is, have the same spectrum $S_0(\omega)$, but one lags the other such that $x_2(t) = x_1(t-T)$, then the cross-spectra are given by

$$S_{x_1 x_2}(\omega) = S_0(\omega)e^{-i\omega T}, \quad S_{x_2 x_1}(\omega) = S_0(\omega)e^{i\omega T}, \tag{30}$$

which also satisfies the general relationship that $S_{x_2x_1}(\omega)$ is always the complex conjugate of $S_{x_1x_2}(\omega)$. Eq. (30) can readily be shown to be true by considering the cross-correlation $R_{x_1x_2}(\tau) = \int_{-\infty}^{\infty} x_1(t)x_2(t-\tau)\,\mathrm{d}t$, the Fourier transform of which (including a factor of $1/2\pi$) gives the cross-spectrum $S_{x_1x_2}(\omega)$.

If the wheels of the trains are assumed to be perfectly smooth, so that all irregularities are contained in the rail surface, the axle inputs can be assumed to differ by a time delay only, giving cross-spectra between inputs of the type in Eq. (30). This assumption ignores the effect of wheel irregularities that are bound to exist on real trains. The wavelengths and amplitude of wheel irregularities, and hence their effective contribution to the total excitation, could be expected to vary with a number of factors, including whether the wheels are tread braked or disc braked. In particular, the existence of wheel irregularities is likely to weaken the degree of coherence between axle inputs that Eq. (30) implies. Nonetheless, the smooth-wheel assumption is a useful starting point for a more realistic input excitation in comparing the effectiveness of various configurations of floating-slab track. The time delay between two adjacent axles is $T = L/v$, where L is the axle spacing (assumed to be constant) and v is the speed of the trains. If the axles are not adjacent, this time delay is multiplied by the integer difference $(q-p)$ between the indices of the two axles concerned. Thus, the general formula (29) for the output spectrum can be written

$$S_y(\omega) = \sum_{p=1}^{N}\sum_{q=1}^{N} H_p^*(\omega)H_q(\omega).S_0(\omega)\mathrm{e}^{-\mathrm{i}\omega(q-p)L/v} \tag{31}$$

assuming that an axle with a higher index is further to the back of the train.

The FRFs $H_p(\omega)$ and $H_q(\omega)$ in Eq. (31) can be obtained from the appropriate elements of the soil-response vector $\mathbf{Y}_3$ in Eq. (27)—which is for an input at the centre axle mass only—by means of the shifting principle. The model should, of course, then include N axle masses instead of just five, and N should be sufficiently large for convergence of the soil responses so that the shifting principle is valid. Strictly, because of the way the FRFs are derived and because the time delays between axles are taken as all the same, result (31) gives the statistical response of a point which moves longitudinally through the soil at the train speed and so stays opposite the axle mass placed at $x = 0$; but it is the vibration level at a stationary observation point next to the tunnel which is of interest. The response of a stationary point will be influenced by Doppler effects, because the wheels at the front of the train and ahead of the point will be moving away from it, while those at the rear of the train and behind the point will be moving towards it, altering the effective time delays. However, Doppler effects are not very significant in this case, because the train speeds (below 30 m/s) are much less than the speeds of pressure and shear waves in the soil (944 and 309 m/s, respectively, for the soil parameters given in Table 1), so can be ignored. A further consideration despite this is whether the total response varies much with the actual longitudinal position of the observation point, next to an axle or somewhere between two axles. In the soil around an actual underground railway system, a hypothetical observer close to the tunnel will "hear" individual axles as they pass, whereas an observer further away will only detect a continuous "rumble" as the train goes by. Thus, if the observation point is at a distance from the tunnel larger than the axle spacing, the point's relative longitudinal position should not have much bearing on the total vibration response perceived. Given these two considerations, result (31) provides a reasonable estimate of the vibration spectrum at a *stationary* observation point in the soil.

The actual input between wheel and rail is a roughness displacement δ which varies along the rail. The spectrum for this would normally be given as a function of wavenumber γ. The roughness spectrum as a function of frequency depends on the speed v of a vehicle traversing the rough surface, and is given by

$$S_\delta(\omega) = \frac{1}{v}\,S_\delta\left(\gamma = \frac{\omega}{v}\right). \tag{32}$$

An important property of the spectrum of a random process $y(t)$ is that integrating it over all frequencies ω gives the expected value of y^2, or mean-square (MS) value of the process, that is

$$\mathrm{MS} = E[y^2] = \int_{-\infty}^{\infty} S_y(\omega)\,\mathrm{d}\omega \tag{33}$$

The widely used root-mean-square (RMS) value of the process is obtained by taking the square root of the MS value (33).

The spectra discussed above are all even (symmetric) functions of angular frequency (or wavenumber), defined for frequencies from $-\infty$ to $+\infty$. However, practical spectra are usually single-sided functions defined for positive frequencies only, with the frequencies themselves in cycles (rather than radians) per unit time (or per unit length). If such single-sided spectra are used, they must still give the MS value when integrated over all frequencies for which they are defined, that is, over 0 to $+\infty$ with a frequency f instead of the angular frequency ω in Eq. (33). Thus a factor of 2 arises from their being single-sided and a factor of 2π from the change to cyclical frequency, giving the single-sided spectrum $S_y(f)$ as

$$S_y(f) = 4\pi S_y(\omega = 2\pi f) \tag{34}$$

and similarly for a single-sided spectrum $S_\delta(1/\lambda)$ of roughness

$$S_\delta\left(\frac{1}{\lambda}\right) = 4\pi S_\delta\left(\gamma = \frac{2\pi}{\lambda}\right), \tag{35}$$

where λ is wavelength. All the relationships given for double-sided spectra still hold if *all* of them are replaced by the equivalent single-sided spectra.

Note also that because the units of a spectrum are (units of y)^2/(units of frequency), it is often more convenient to plot graphs of root spectrum with units of (units of y)/$\sqrt{\text{units of frequency}}$, to reduce the range of values of the spectrum. The results from the full-track model will be plotted as root spectra.

4.4. Results for the tunnel with a full-track model

As for the simple-slab model, the tunnel and soil FRFs were calculated as described briefly in Section 2, using the parameters in Table 1. The parameter values for the full track are given in Table 3. The slab properties used are the same as those for the simple-slab model given in Table 2, including the three different slab-support stiffnesses and loss factor. The rail beam represents the two rails together, and with the rail pad stiffness gives a resonance of the rail on the rail pads of 318 Hz, above the 200 Hz maximum frequency considered here. Results were calculated using an inverse FFT of 2048 points with a sampling interval of $\Delta x = 0.5$ m, as for previous results. This gives a maximum x-value of 512 m, so the maximum longitudinal separation which can be used with the shifting principle to create the FRF matrices such as Eq. (24) is also 512 m; all the axle masses must therefore fit within this distance. With a regular spacing of $L = 20$ m, the maximum odd number of axles (odd to retain symmetry about $x = 0$) which can be added is thus $N = 25$. This number of axles gave converged soil responses for a roughness input at the $x = 0$ axle mass.

Due to the cylindrical geometry of the tunnel-in-soil model, the displacement is expressed as longitudinal, tangential and radial components U, V and W (see Fig. 1). However, horizontal and vertical components are more meaningful when considering inputs to building foundations, so an absolute coordinate system XYZ needs to be defined. The longitudinal direction X coincides with the longitudinal x-axis of the tunnel, the horizontal direction Y with the $\theta = 90^\circ$ radius, and the vertical direction Z with the $\theta = 180^\circ$ radius. Thus the relationships of the new longitudinal, horizontal and vertical displacement components U_X, U_Y and U_Z to the

Table 3
Parameter values for the various parts of the full track

Slab beam	Rail beam	Axle masses
$EI = 1430 \times 10^6$ Pa m^4	$EI_r = 10 \times 10^6$Pa m^4	$m_a = 500$ kg
$m = 3500$ kg/m	$m_r = 100$ kg/m	$N = 25$
$k = 1262 \times 10^6$ N/m^2(60 Hz)	$k_r = 400 \times 10^6$ N/m^2	$L = 20$ m
$k = 424.4 \times 10^6$ N/m^2(45 Hz)	$\eta_{kr} = 0.3$	
$k = 146.6 \times 10^6$ N/m^2(30 Hz)		
$\eta_k = 0.5$		

The three different slab-support stiffnesses are the same as those given in Table 2 for the simple slab.

original components U, V and W are

$$U_X = U, \quad U_Y = V\cos\theta - W\sin\theta, \quad U_Z = V\sin\theta + W\cos\theta. \tag{36}$$

The FRFs can be calculated for the U, V and W components of soil displacement, then resolved according to Eq. (36) before being used in the PSD Eq. (31).

A useful way to evaluate the effect of floating the track slab is to take the ratio of the soil responses with and without resilient bearings inserted between the slab and tunnel invert. A common measure of this ratio is the "Insertion Loss" in dB, which gives the amount of *reduction* in vibration provided by the bearings, so Insertion Losses greater than zero indicate vibration isolation. However, this notion is opposite to all the results presented so far, where a higher (absolute) response is worse. To maintain consistency, the concept of "Insertion Gain" in dB, indicating the *increase* in vibration levels caused by the bearings (hence the negative of Insertion Loss), will be used here; it is increasingly being used in industry (see Greer and Manning [11] for example). The definition of Insertion Gain for the current results is

$$\text{Insertion Gain [dB]} = 20\log_{10}\sqrt{\frac{S_j|_{f_n}}{S_j|_{\text{direct}}}}, \quad j = X, Y \text{ or } Z, \tag{37}$$

that is, the ratio of the soil-displacement root spectrum for a slab "natural frequency" of f_n to the root spectrum for a model with a directly joined slab. Insertion Gains less than zero indicate vibration isolation.

The computation procedure for calculating the PSDs of soil displacement for the full-track model can be summarised as follows:

1. Join the slab beam to the tunnel by Eqs. (9) or (11) for each slab-support stiffness k, join the rail beam to the slab by Eq. (18), and obtain the rail FRF (21) by inverse FFT.
2. Obtain the rail dynamic-stiffness matrix via the FRF matrix (24), add axle masses according to Eq. (26), and use the resulting displacement vector to calculate the rail interaction forces from Eq. (25).
3. For each radius r and angular position θ of interest for the soil:
   (i) Calculate the soil FRFs for the uncoupled tunnel by summing the appropriate modes for n from 0 to 10 according to Eq. (3).
   (ii) Add the effect of the slab beam by Eq. (12) and that of the rail beam by Eq. (19), then obtain the soil FRF (22) for a tunnel with a floating-slab track by inverse FFT.
   (iii) Form the soil FRF matrix and obtain the soil displacement vector from Eq. (27) and the interaction forces calculated above.
   (iv) Calculate the soil PSDs for this position from Eq. (31) for each train speed v required.

The PSDs for different slab-support stiffnesses can then be used to calculate Insertion Gains from Eq. (37) or RMS levels via the MS (33).

Once again, symmetry can be used to reduce the computation required. The longitudinal symmetry means that ξ-domain displacements need only be calculated at the 1025 points with $\xi \geqslant 0$, with the rest of the sample being created by a suitable reflection just prior to the inverse FFT; and symmetry about the vertical centreline of the tunnel cross-section means that only soil positions within the range $0 \leqslant \theta \leqslant 180^\circ$ need to be considered. Nevertheless, the arrays representing modal displacements as functions of ξ and ω at a given radius r, which are summed together to give the total displacements, still require large amounts of memory. This means that careful management of data swapping between disk and memory is needed.

Spectra were computed for a "white" (uniform) input roughness spectrum of $S_0 = 1\,\text{mm}^2/\text{Hz}$ in Eq. (31). This gives equal weighting to all frequencies. Although a uniform roughness spectrum is unrealistic, it does show the fundamental transmission behaviour of the track–tunnel–soil system. It is clear from Eq. (31) that the output PSD for a non-uniform input is obtained simply by multiplying the uniform result by the actual input $S_0(\omega)$, which is independent of the summation. This also means that the Insertion Gain (37) is independent of the details of input, as $S_0(\omega)$ will cancel in the ratio of the two output spectra.

Figs. 16–18 give contour plots of the longitudinal, horizontal and vertical PSDs, respectively, at a radius of 20 m and a train speed of 40 km/h, on axes of frequency versus angular position. Graph (a) in each figure

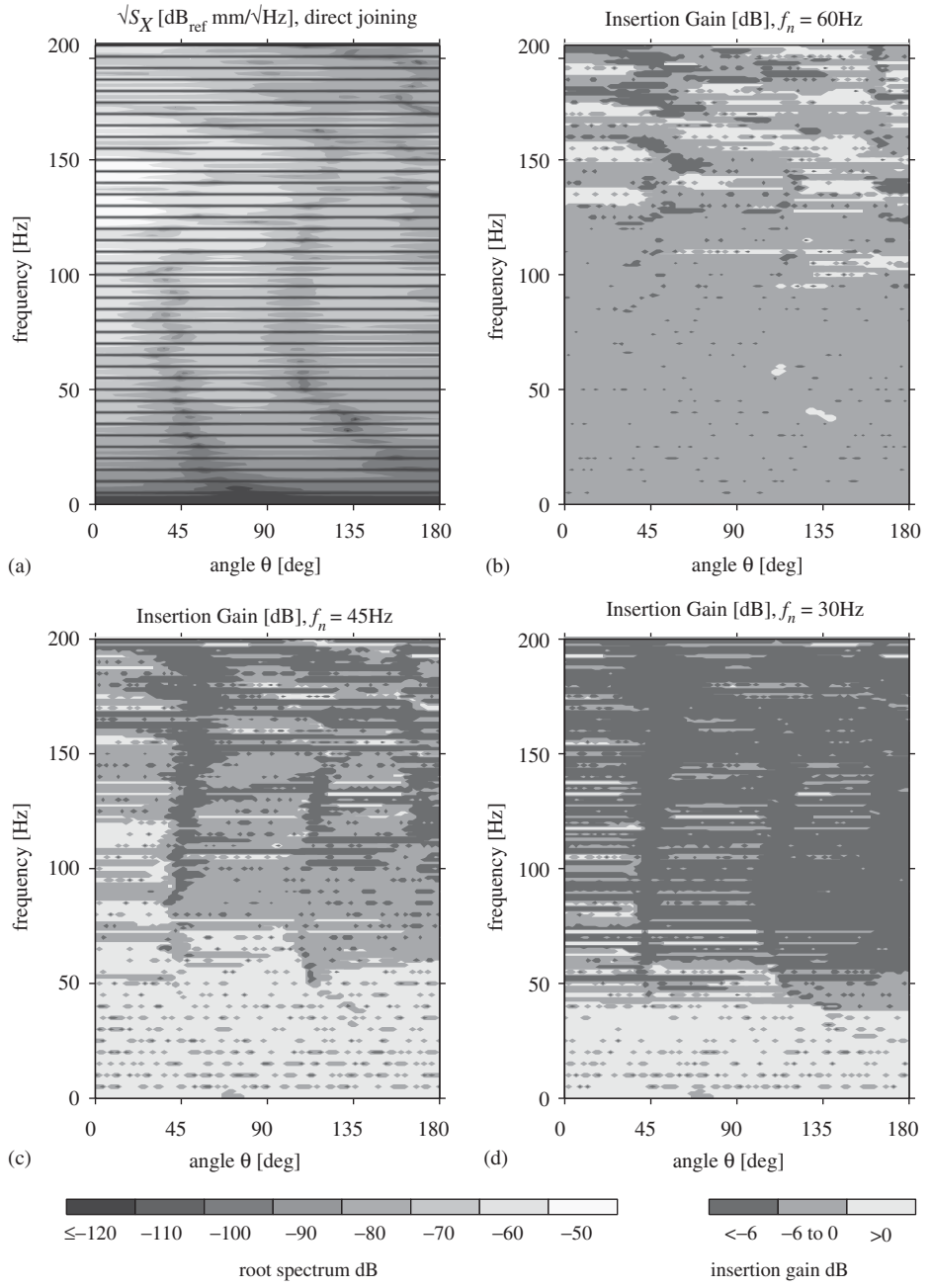

Fig. 16. (a) Longitudinal soil displacement spectrum for a full-track model joined directly to the tunnel invert and (b)–(d) Insertion Gains relative to (a) with increasingly softer slab-support stiffnesses, at a radius of 20 m with a train speed of 40 km/h. $\theta = 0$ is directly underneath the tunnel invert and $\theta = 180^\circ$ is directly above the tunnel. White (uniform) input roughness spectrum of $1\,\mathrm{mm}/\sqrt{\mathrm{Hz}}$ between rail and wheel.

shows the soil displacement spectrum for a white input when the slab is joined directly to the tunnel invert. The contour intervals are 10 dB, centred on the values given in the legend. Graphs (b)–(d) show the Insertion Gains for the three slab-support stiffnesses given in Table 3. The Insertion Gains are presented as "acceptability" plots, with just three levels: <6 dB indicates effective isolation, -6 to 0 dB indicates only marginal reduction in soil vibration, and >0 dB indicates performance worse than a directly joined slab. The small improvements represented by marginal reduction may not be worth the cost of floating the track slab.

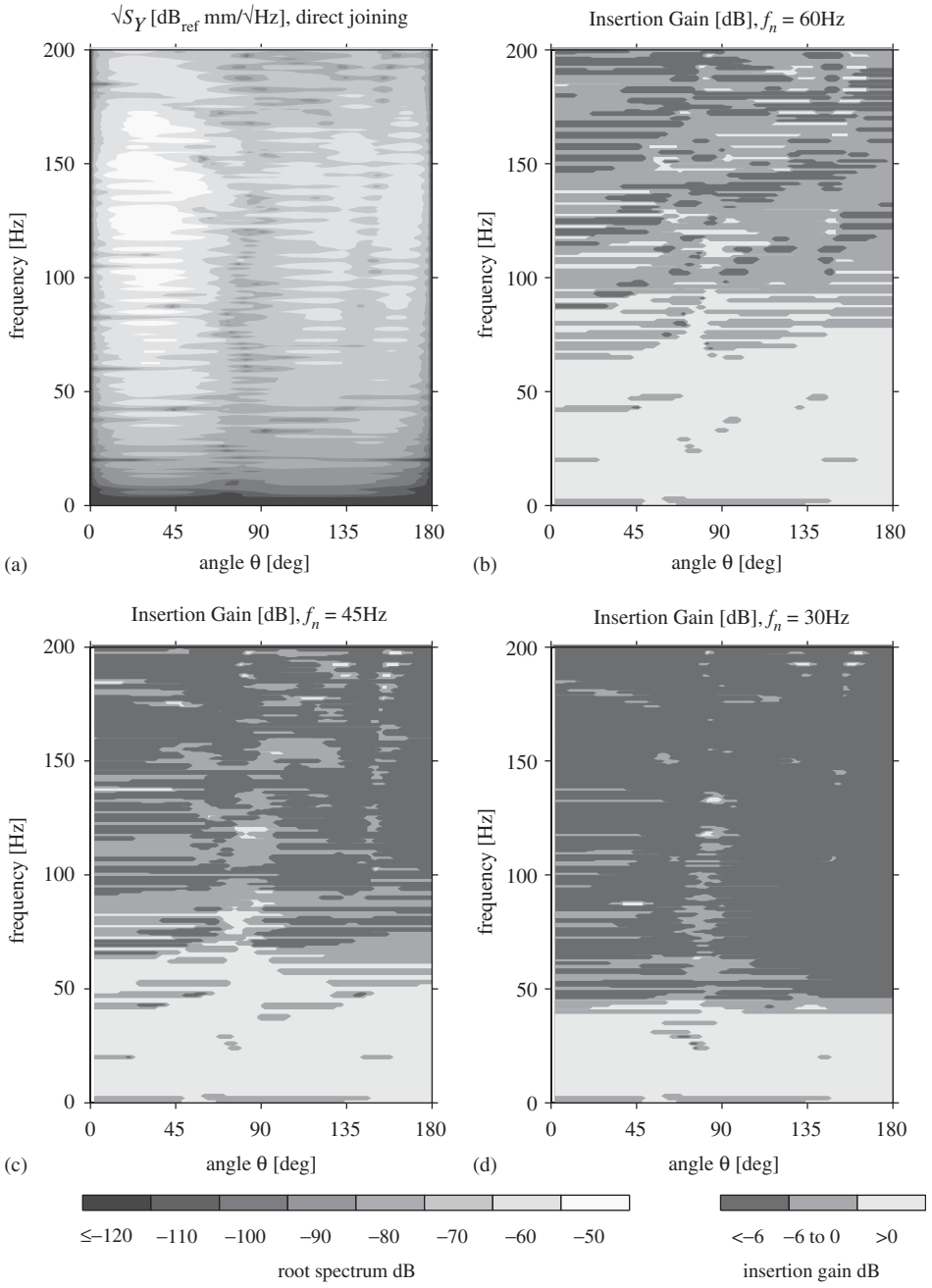

Fig. 17. (a) Horizontal soil displacement spectrum for a full-track model joined directly to the tunnel invert and (b)–(d) Insertion Gains relative to (a) with increasingly softer slab-support stiffnesses, at a radius of 20 m with a train speed of 40 km/h. Otherwise as for Fig. 16.

The three spectra (a) in Figs. 16–18 for a directly joined slab beam have some common features. The soil vibration levels for frequencies below 10 Hz are all very small compared to the rest of the frequency range, and because the Insertion Gains (b)–(d) in each figure are all near 0 dB below 10 Hz, this can also be said for the slabs supported on varying stiffness. Since all input frequencies have equal weighting, this shows that very low frequencies are highly attenuated by the track–tunnel–soil system; therefore, the assumption that these frequencies are relatively insignificant is justified. Maximum activity occurs between 100 and 160 Hz, but

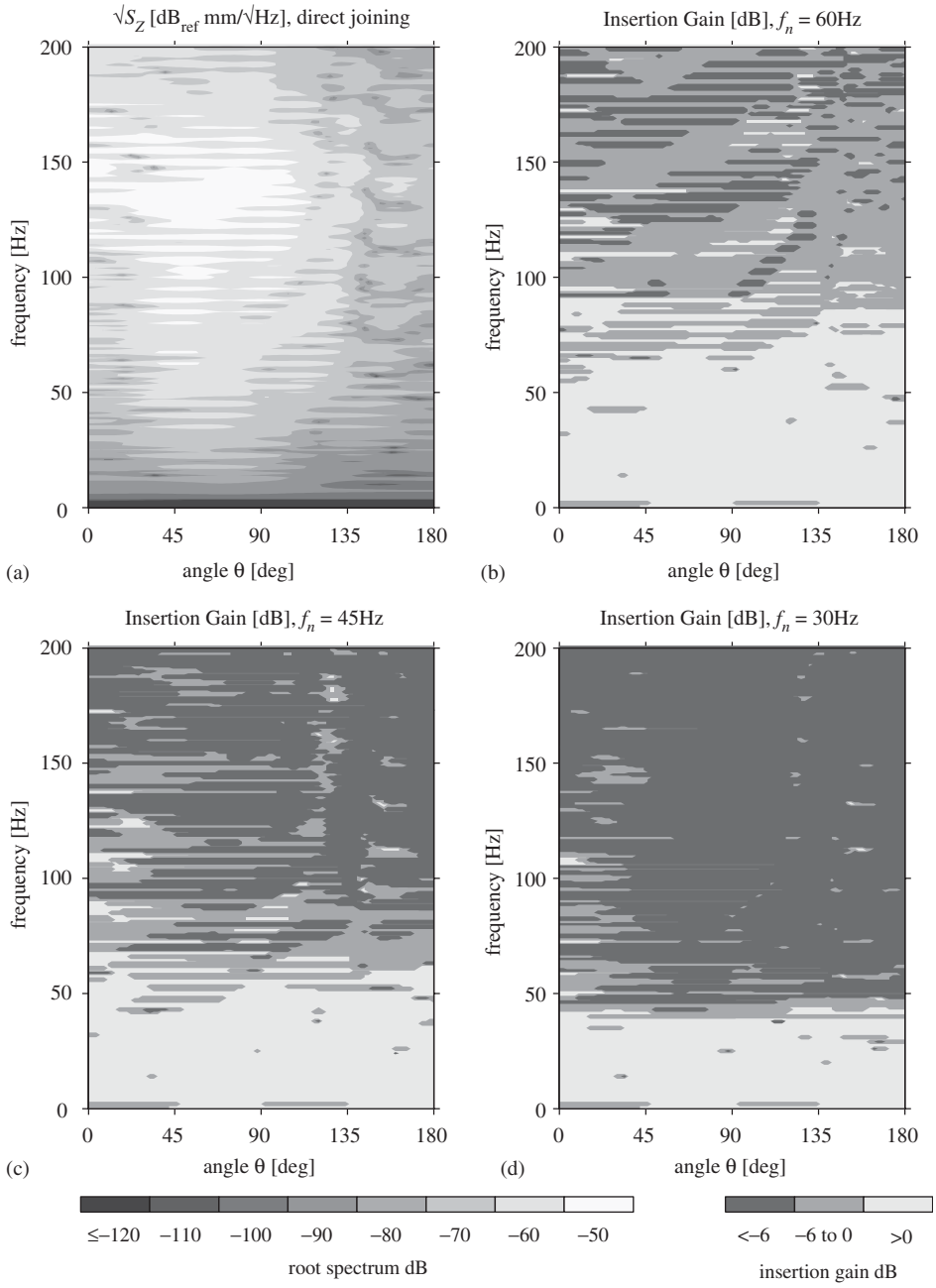

Fig. 18. (a) Vertical soil displacement spectrum for a full-track model joined directly to the tunnel invert and (b)–(d) Insertion Gains relative to (a) with increasingly softer slab-support stiffnesses, at a radius of 20 m with a train speed of 40 km/h. Otherwise as for Fig. 16.

longitudinal levels seem to be lower than horizontal and vertical ones. The highest levels occur mainly for angular positions less than 100°, underneath and to the sides of the tunnel, resulting in a "vibration shadow" in the soil above the tunnel. The vibration shadow is probably beneficial, if a high proportion of energy propagated downwards means propagation away from nearby building foundations. The Insertion Gain plots (b), (c) and (d) are for increasingly softer resilient bearings with designed natural frequencies of 60, 45 and 30 Hz. This gives $\sqrt{2}f_n$ frequencies, above which isolation is supposed to occur, of 84.9, 63.6 and 42.4 Hz,

respectively. Insertion Gains are generally positive until the $\sqrt{2}f_n$ frequencies, but do not become uniformly negative above these—there are many pockets of increased response at higher frequencies. Clearly, simple vibration-isolation theory is not applicable in the current situation.

Each displacement component has some individual characteristics. Fig. 16(a) for the longitudinal PSD has a series of very deep troughs at 5 Hz intervals. It is not clear how these deep antiresonances arise. The antisymmetric nature of the FRF for longitudinal displacement does not fundamentally alter the way the terms in the PSD summation (31) add up compared to the symmetric FRFs for the horizontal and vertical displacement components. The antiresonances cannot be due to standard wheelbase filtering, because they were found to appear at the same 5 Hz intervals regardless of train speed. Further investigation is required to determine the mechanism responsible for this regular attenuation. The many small, round contours in Figs. 16(b)–(d) giving a ''dotted'' appearance are most probably due to numerical fluctuation in the Insertion Gain ratio of the very small magnitudes at the trough frequencies, so should be ignored. Nevertheless, Figs. 16(b) and (c) show that insertion of only a small amount of resilience gives only marginal vibration reduction over the whole frequency range, with some positions showing increases right up to 200 Hz when the slab is floated. The softest mounting, Fig. 16(d), gives worthwhile reductions for many soil positions above 70 Hz, but this is much higher than the corresponding $\sqrt{2}f_n$ value of 42.4 Hz and there are still significant areas of increased response.

The spectrum of horizontal displacement, Fig. 17(a), has minima at $\theta = 0^\circ$ and at 180°, since the horizontal displacement at these two positions, as given by Eq. (36), is wholly made up of the tangential component V, which is zero directly above and below the tunnel. There are high levels of vibration for a wider frequency range than the longitudinal displacement. Clearly discernible are horizontal fingers in the contours, indicating undulation in the surface represented by the contour plot. The most obvious frequency spacing from crest to crest is about 5 Hz, although closer inspection reveals smaller spacing on some parts of the surface. This undulation arises from wheelbase filtering, due to coincidence of roughness wavelength with the axle spacing on the track: crests occur when all the axle masses move up and down in phase, troughs when they move out of phase. For the train speed of 40 km/h (11.1 m/s) and axle spacing of 20 m, the expected frequency interval between peaks of in-phase force transmitted to the tunnel invert is 0.556 Hz. This is not discernible in Fig. 36(a) for two reasons. Firstly, the contour interval of 10 dB will not show many surface undulations of smaller magnitude. Secondly, the spectrum results were computed for a frequency step of 1 Hz, which is a resolution too coarse to show variation at a period of 0.556 Hz. Thus, the variation can only be seen at a multiple of the fundamental frequency interval. The Insertion Gains, Figs. 17(b)–(d), show the same kind of behaviour as Fig. 16 when the slab bearings become softer, but there are now more positions that have significantly reduced vibration levels. The positions above the $\sqrt{2}f_n$ frequencies with increased vibration are concentrated around $\theta = 90^\circ$, the horizontal plane bisecting the tunnel. Once again, largely beneficial results are only achieved with the softest slab bearings, Fig. 17(d).

The spectrum of vertical displacement, Fig. 18(a), is similar to the horizontal one in Fig. 17(a), showing the same surface undulation due to wheelbase filtering. However, the highest levels of vibration extend further around the tunnel, from directly underneath to more than 90°. The Insertion Gains follow a similar pattern too, although Fig. 18(d) shows that the softest bearings reduce vertical vibration more than the horizontal vibration of Fig. 17(d). The positions with increased vibration above the $\sqrt{2}f_n$ frequencies are now concentrated near $\theta = 0$, underneath the tunnel. This, with the $\theta = 90^\circ$ concentration for increased horizontal vibration, suggests that the radial component W of soil vibration is not well attenuated and is even increased by the addition of resilient slab support.

PSDs can be calculated for other soil radii and train speeds to determine the effects these parameters have. This is done for the vertical component of displacement in the thesis [45]. Higher maximum levels occur when closer to the tunnel, because there has been less geometric spreading and less damping of vibrational energy. Varying the speed changes the spacing of the wheelbase-filtering contour fingers, so that lower speeds split the areas into more fingers and higher speeds cause separate fingers to coalesce into wider ones. However, the general characteristics of the spectra and Insertion Gains remain much the same.

Although it is informative to plot the response of the full-track model to a white roughness input spectrum, ultimately the soil vibration levels induced by actual wheel–rail roughness need to be known. Frederich [52] gives a formula for rail irregularity PSDs based on many measurements of the track geometry of different

Table 4
Values of the unevenness a and waviness b of vertical railway track irregularity, for three different track conditions

	a (mm^2.(1/m)^2)	b (1/m)
Worst	9.39×10^{-1}	6.89×10^{-2}
Average	1.31×10^{-2}	2.94×10^{-2}
Best	1.90×10^{-4}	9.71×10^{-3}

From Frederich [52].

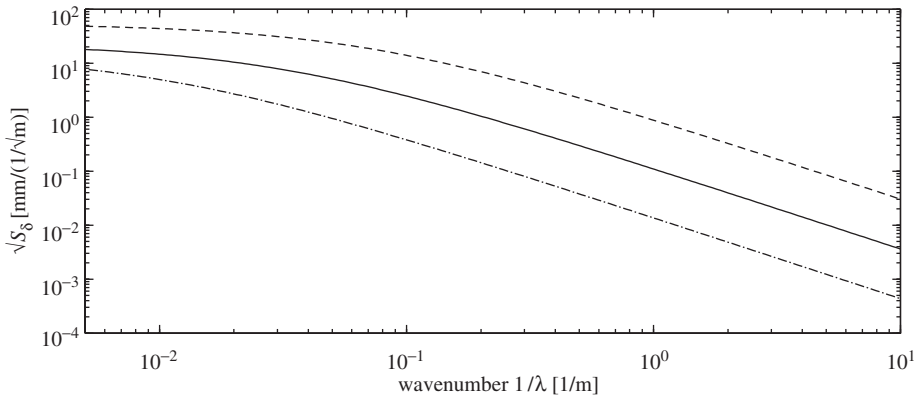

Fig. 19. Spectrum of vertical rail irregularity versus wavenumber of the irregularity for railways in worst ----, average — and best ·-·-·- condition. Plotted from Eq. (38) using the parameters of Table 4. Based on Frederich [52].

surface railways. The spatial PSD of track irregularity is given by the single-sided spectrum

$$S_\delta\left(\frac{1}{\lambda}\right) = \frac{a}{(b + 1/\lambda)^3}, \tag{38}$$

where λ is the irregularity wavelength, a is an "unevenness" parameter and b is a "waviness" parameter. The values of a and b for irregularity in the vertical height of the rails are given in Table 4. The parameters for track in "worst" and "best" condition define the envelope of all measured data. Formula (38) is valid for wavelengths λ from 0.1 to 200 m; smaller wavelengths are due to rail surface roughness and larger ones to variations in the topography of the ground surface. Function (38) is plotted in Fig. 19 for the three track conditions described by the parameters in Table 4.

To convert the PSD (38) to a function of frequency f, relation (32) is applied, recalling that $1/\lambda = f/v$ where v is the train speed, to give the single-sided roughness spectrum

$$S_\delta(f) = \frac{1}{v}\frac{a}{(b + f/v)^3}, \tag{39}$$

which can be used as S_0 in Eq. (31). Function (39) is plotted in Fig. 20 for a track in average condition, for three different train speeds. The frequencies below 20 Hz (corresponding to long wavelengths) receive a very high weighting. Note that to cover frequencies up to 200 Hz, Eq. (39) is extrapolated below the 0.1 m minimum wavelength (frequencies greater than 56 Hz at 20 km/h and 111 Hz at 40 km/h) for which the function was originally defined. It is arguable whether rail surface roughness and corrugation has a smaller (as given by the extrapolation in Fig. 20) or comparable magnitude to small-wavelength irregularity in the track geometry.

The actual spectra of soil vibration are obtained by multiplying the previously calculated spectra for a white input by S_δ of Eq. (39) according to the PSD formula (31). Although Fig. 20 shows a large bias in the input towards low frequencies, the overall effect of multiplying it with the PSDs calculated for a white input is

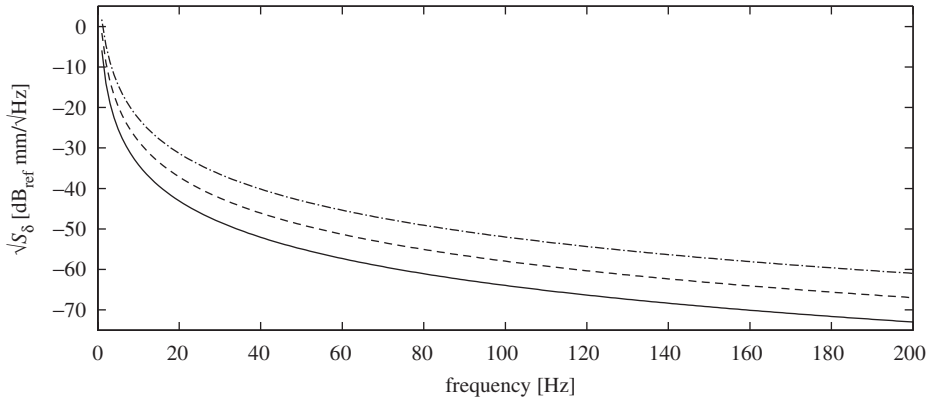

Fig. 20. Spectrum of vertical rail irregularity versus frequency for railway in average condition, calculated for three different train speeds (20 km/h —; 40 km/h - - - -; and 80 km/h · - · - · -) from Eq. (39) and corresponding to the "average" curve of Fig. 19. Note that this is an extrapolation on Frederich's [52] data for $f > 56$ Hz when $v = 40$ km/h and for $f > 111$ Hz when $v = 40$ km/h.

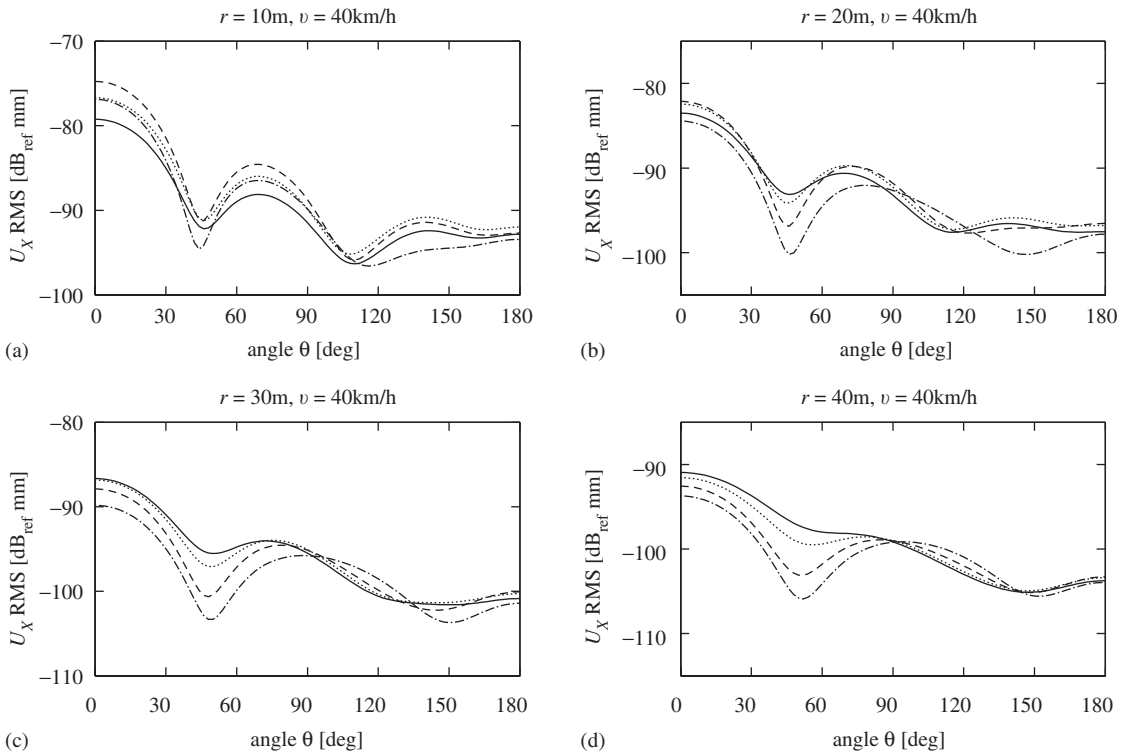

Fig. 21. Longitudinal soil displacement RMS levels for a train speed of 40 km/h, around the tunnel at radii of (a) 10 m, (b) 20 m, (c) 30 m and (d) 40 m. $\theta = 0$ is directly underneath the tunnel invert and $\theta = 180^\circ$ is directly above the tunnel. Calculated with the realistic roughness input spectrum of Fig. 20 for direct joining —— of the slab and 60 Hz ·····, 45 Hz - - - - - - and 30 Hz - · - · - · - support stiffnesses.

simply to flatten out each spectrum over the whole frequency range, because those PSDs have very low levels at low frequencies. Nevertheless, if the extrapolated rail-roughness magnitude above 111 Hz for 40 km/h is indeed underestimated, then the spectra could be increased by up to 7 dB for the highest frequencies considered.

The RMS levels of soil vibration are obtained by integrating the spectra for a realistic input, using the MS (33). Each spectrum surface is thus condensed to a single curve which is a function of angular position. Fig. 21 shows the effect of resilient slab bearings on the RMS level of longitudinal soil vibration at various radii for a train speed of 40 km/h. Close to the tunnel at 10 m radius, the effect of adding resilience is to increase the RMS level at most positions around the tunnel, with only the softest bearings giving a reduction for angles greater than 120°, above the tunnel. As the radius is increased, the levels for angles less than 90° drop below the directly joined case, but this is all under the tunnel and thus not so important. At angles corresponding to positions above the tunnel, adding resilience generally increases the levels by a few dB, with a marginal improvement provided at some positions again only by the softest bearings. Note that the variation about the levels for the directly joined slab are all within about ± 5 dB, which is not very much compared to the tens of dB reduction that would be predicted by a simple mass–spring model.

The RMS levels of horizontal displacement in Fig. 22 show that at 10 m radius, this component behaves in a way opposite to the longitudinal one. Any amount of resilience reduces vibration at most positions, with the softest giving up to 7 dB reduction. But this effect is diminished as the radius increases, with all responses collapsing on to that for the directly joined slab at 40 m radius, the vibration for angles greater than 90° even being slightly increased. A similar picture emerges from the RMS levels of vertical soil displacement shown in Fig. 23. As for the original PSDs, the horizontal and vertical RMS levels are generally higher than the longitudinal one. The changes with radius in the relative levels produced by different amounts of resilience may be explained by varying proportions of shear-wave energy and pressure-wave energy being induced in the soil in each case. Because the soil material damping acts in shear, it will only attenuate shear-wave energy and not pressure-wave energy, while both are subject to radiation damping due to geometric spreading with increasing radius. It is perhaps the case that a closely coupled slab beam induces more soil shear motion that contributes to horizontal and vertical displacement than one on softer springs, so that the effect of material damping is correspondingly more, eventually reducing responses for all slab-support stiffnesses to similar levels at large radius. The opposite effect in the longitudinal component may indicate that a *less* closely

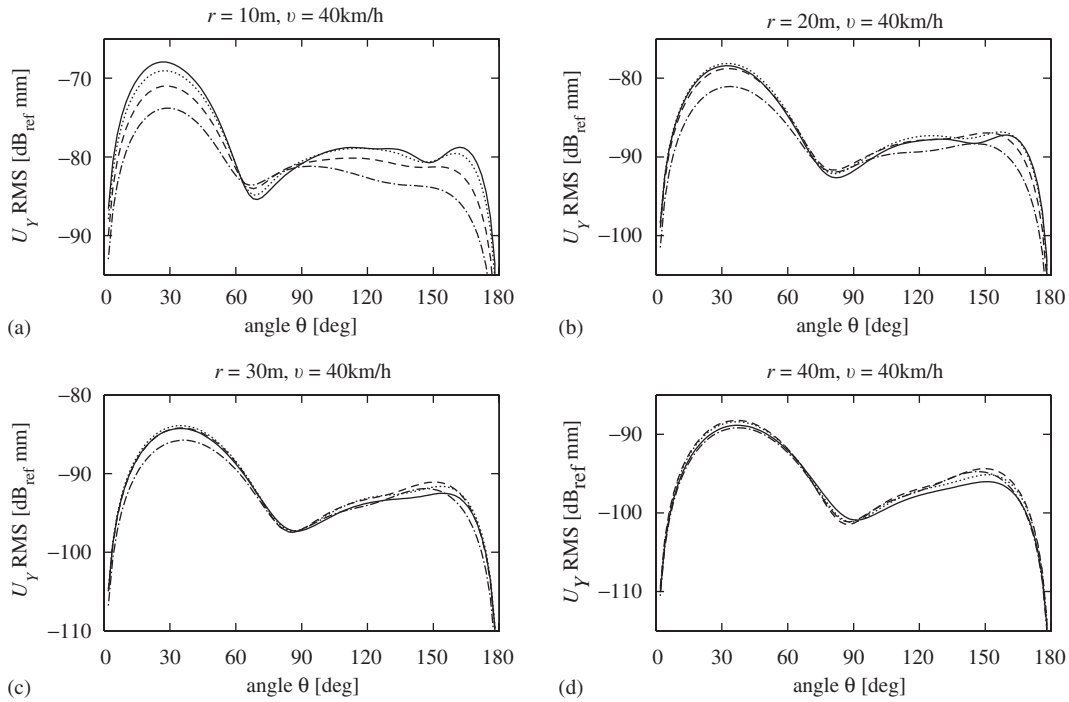

Fig. 22. Horizontal soil displacement RMS levels for a train speed of 40 km/h, around the tunnel at radii of (a) 10 m, (b) 20 m, (c) 30 m and (d) 40 m, calculated for direct joining —— and 60 Hz ·····, 45 Hz - - - - - - and 30 Hz ·····support stiffnesses. Otherwise as for Fig. 21.

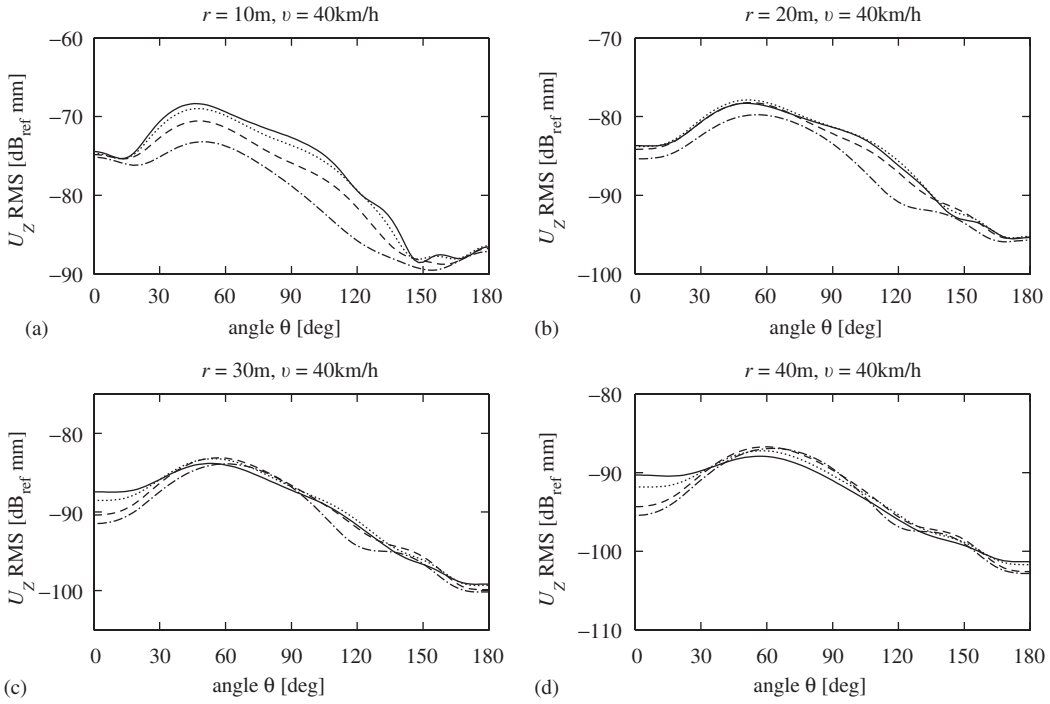

Fig. 23. Vertical soil displacement RMS levels for a train speed of 40 km/h, around the tunnel at radii of (a) 10 m, (b) 20 m, (c) 30 m and (d) 40 m, calculated for direct joining —— and 60 Hz ·····, 45 Hz - - - - - - and 30 Hz ·····- · - · ····· support stiffnesses. Otherwise as for Fig. 21.

coupled slab induces more shear motion in directions that contribute strongly to longitudinal displacement. For an observation point in the soil directly opposite a single load on the track, shear motion in the plane of the tunnel cross-section will only contribute to the observed horizontal and vertical displacements, while shear motion normal to that plane will only contribute to the observed longitudinal displacement. It might be expected that the effects observed in the RMS responses due to the multiple axle inputs considered here would be dominated by the axle nearest, and thus directly opposite, the observation point. This would imply that softer slab bearings result in less energy propagated as cross-sectional-plane shear waves but more energy as normal-plane ones. The situation is complicated by the fact that the transmission paths from the vicinities of the axles to the observation point at a given angular position are not the same for different radii. Additionally, the alignment of the horizontal and vertical components relative to the radiating tunnel varies with angular position. The longitudinal position of the observation point relative to the axle stations spaced at 20 m could also be significant, especially for smaller radii.

Fig. 24 shows the effect of doubling the train speed on the RMS levels of vertical displacement. The graphs are almost identical in shape to those in Fig. 23; they are just increased uniformly by about 5 dB. Similarly, halving the speed was found to decrease all levels by about 5 dB. This is true for the other two displacement components as well. This follows from the similarity of the curves in Fig. 20 for the input spectrum at different speeds, and the observation that train speed does not change the general distribution of vibration level with respect to frequency and angular position. Thus, the maximum achievable reduction in RMS levels is of the order of only 6 dB regardless of train speed.

5. Conclusions

A track slab can be modelled by a bending beam coupled to the tunnel, either directly or via resilient bearings, using straightforward algebra in the wavenumber domain. This simple model demonstrates that Winkler-beam theory is inadequate for the design of floating-slab track. While the driving-point response of a

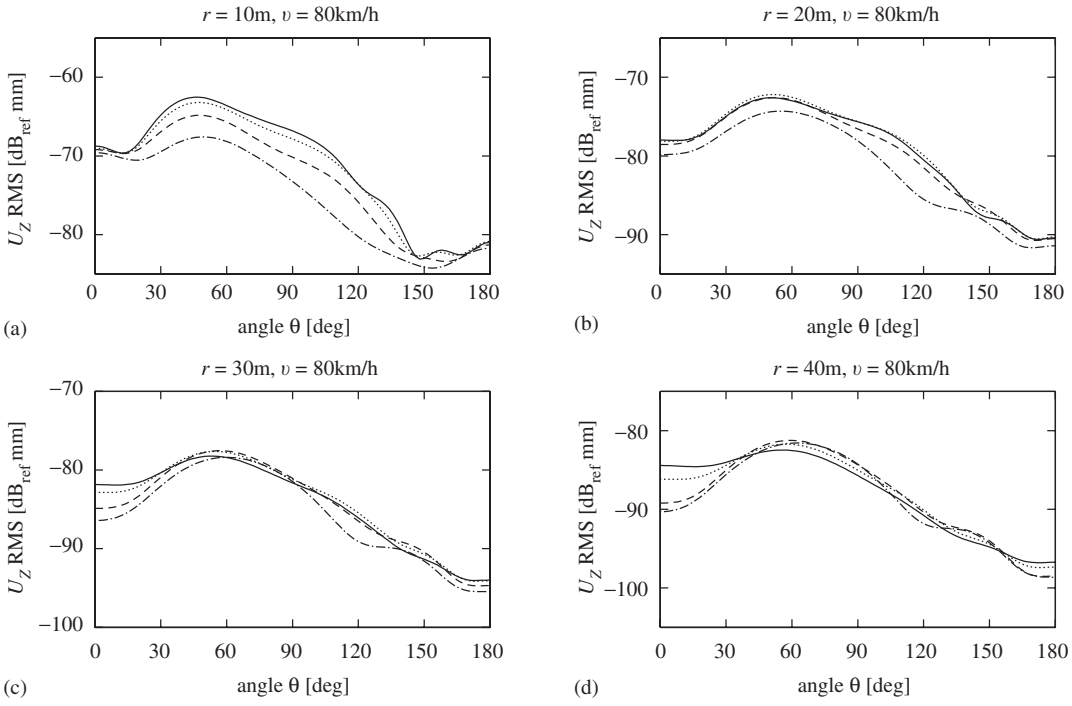

Fig. 24. Vertical soil displacement RMS levels for a train speed of 80 km/h, around the tunnel at radii of (a) 10 m, (b) 20 m, (c) 30 m and (d) 40 m, calculated for direct joining —— and 60 Hz ·····, 45 Hz - - - - - - and 30 Hz·····- - - support stiffnesses. Otherwise as for Fig. 21.

slab on soft bearings is passably well modelled by a Winkler beam, radiation of energy into the soil heavily attenuates the response of slab beams more closely coupled to the tunnel. The tunnel also transmits energy to the slab beam at points away from the load at low frequencies, whereas a Winkler beam cannot do this below its ''natural frequency'', which marks the onset of travelling waves. Mounting the track slab on resilient bearings allows energy to propagate down the slab before being transmitted to the tunnel then soil, so that under the slab load, the tunnel invert response is decreased compared to a directly joined slab beam, but is increased at positions further down the tunnel. This is reflected in the soil displacements, for which resilient bearings produce responses like classic vibration isolation for positions next to the slab load, but higher levels at other longitudinal positions.

A complete track model can be constructed by adding a rail beam to the slab-plus-tunnel model using the same original wavenumber-domain coupling equations, then adding axle masses via an FRF matrix for the rail. For a model of infinite length, a shifting principle can be invoked to calculate the soil response due to inputs at every train axle by considering responses to only one input at the middle axle. Contour plots of soil displacement PSDs for uniform random roughness-displacement inputs between the axles and the rail show that the track–tunnel–soil system considered attenuates frequencies below 10 Hz the most and frequencies between 100 and 160 Hz the least. The highest levels occur under and to the sides of the tunnel, resulting in a vibration shadow above the tunnel. Longitudinal vibration levels are less overall than horizontal and vertical ones. The differences between these three components prompt the question of which ones are the most important in transmitting vibration into building foundations. Insertion Gain plots for increasingly softer slab-support stiffnesses confirm that isolation is not achieved at frequencies as low as predicted by simple theory. Any reductions are modest and there are some positions around the tunnel for which resilient slab bearings cause increased response at higher frequencies.

RMS vibration levels can easily be calculated from the PSDs. This was done using a realistic input spectrum giving higher weighting to longer wavelengths of track irregularity. For the system parameters used, floating the track slab increases longitudinal RMS levels near the tunnel, but decreases them at greater radii for some

positions under the tunnel. Resilient bearings reduce horizontal and vertical RMS levels close to the tunnel, but make little difference at large radii. This suggests a complex interplay of differing proportions of pressure-wave and shear-wave energy being induced by the use of different slab-support stiffnesses, with shear-wave energy being attenuated by the soil-damping mechanism assumed. Doubling the train speed simply increases all RMS levels uniformly by approximately 5 dB. Any vibration reduction achieved is modest, no more than 6 dB with the softest slab bearings. Indeed, floating the track slab causes increased transmission of vibration to some positions around the tunnel under certain conditions. This is something that could be investigated further with a wider range of track and soil parameters using the model demonstrated in this paper.

Acknowledgement

The work described in this paper was undertaken while the first author was a doctoral candidate at the University of Cambridge supported by a Cambridge Commonwealth Trust scholarship and Overseas Research Students Award.

References

[1] J.A. Forrest, H.E.M. Hunt, A three-dimensional tunnel model for calculation of train-induced ground vibration, *Journal of Sound and Vibration*, this issue (doi:10.1016/j.jsv.2005.12.032).
[2] C. Esveld, *Modern Railway Track*, Esveld Consulting Services, Zaltbommel, Netherlands, 1989.
[3] W.D. Henn, System comparison: ballasted track–slab track, *Rail Engineering International Edition* (1993) 6–9.
[4] ORE D 151 Specialists Committee, An assessment of vibration counter-measures in current use, Question D 151: Vibrations transmitted through the ground, Report 2, Office for Research & Experiments of the International Union of Railways, Utrecht, Netherlands, 1982.
[5] A. Zach, G. Rutishauser, Measures against structure borne noise and vibrations: experience from projects carried out by Swiss Federal Railways (SBB), Report DT 217, Office for Research and Experiments of the International Union of Railways, Utrecht, Netherlands, 1989.
[6] R. Wettschureck, U.J. Kurze, Insertion loss of ballast mats, *Acustica* 58 (1985) 177–182.
[7] R. Wettschureck, Vibration and structure-borne noise insulation by means of cellular polyurethane (PUR) elastomers in railway track applications, *Rail Engineering International Edition* (1995) 7–14.
[8] R. Wettschureck, Measures to reduce structure-borne noise emissions induced by above-ground open railway lines, *Rail Engineering International Edition* (1997) 12–16.
[9] G.P. Wilson, H.J. Saurenman, J.T. Nelson, Control of ground-borne noise and vibration, *Journal of Sound and Vibration* 87 (1983) 339–350.
[10] G. Capponi, M.H. Murray, Reducing vibration in urban rail transport, *Transactions of Mechanical Engineering IEAust* ME23 (1998) 43–45.
[11] R.J. Greer, C.J. Manning, Vibration isolation for railways, *Acoustics Bulletin* 23 (1998) 13–17.
[12] Z. Cai, G.P. Raymond, R.J. Bathurst, Natural vibration analysis of rail track as a system of elastically coupled beam structures on Winkler foundation, *Computers and Structures* 53 (1994) 1427–1436.
[13] Z. Cai, G.P. Raymond, Use of a generalized beam/spring element to analyze natural vibration of rail track and its application, *International Journal of Mechanical Sciences* 36 (1994) 863–876.
[14] F. Cui, C.H. Chew, The effectiveness of floating slab track system—part I: receptance methods, *Applied Acoustics* 61 (2000) 441–453.
[15] D.J. Mead, Y. Yaman, The response of infinite periodic beams to point harmonic forces: a flexural wave analysis, *Journal of Sound and Vibration* 144 (1991) 507–530.
[16] A. Nordborg, Vertical rail vibrations: pointforce excitation, *Acustica* 84 (1998) 280–288.
[17] A. Nordborg, Vertical rail vibrations: parametric excitation, *Acustica* 84 (1998) 289–300.
[18] L. Gry, C. Gontier, Dynamic modelling of railway track: a periodic model based on a generalized beam formulation, *Journal of Sound and Vibration* 199 (1997) 531–558.
[19] G. Samavedam, P. Cross, Dynamic analyses of vibration isolating tracks for tunnels, Report TN TS 38, Railway Technical Centre, British Rail Research, Derby, England, 1980.
[20] J.A. Forrest, Floating slab railway track for isolation of vibration: models of infinite length, in: *ASME 1997 Design Engineering and Technical Conferences (DETC '97)*, American Society of Mechanical Engineers, Sacramento, USA, 1997.
[21] P.M. Belotserkovskiy, Forced oscillations of infinite periodic structures. Applications to railway track dynamics, *Vehicle System Dynamics Supplement* 28 (1998) 85–103.
[22] K. Ono, M. Yamada, Analysis of railway track vibration, *Journal of Sound and Vibration* 130 (1989) 269–297.
[23] K. Knothe, Y. Wu, Receptance behaviour of railway track and subgrade, *Archive of Applied Mechanics* 68 (1998) 457–470.
[24] H. Kruse, K. Popp, The influence of wave propagation in the subsoil on the train–track dynamics, in: N. Chouw, G. Schmid (Eds.), *Wave 2000—Wave Propagation—Moving Load—Vibration Reduction*, A.A. Balkema, Bochum, Germany, 2000, pp. 171–184.

[25] C.J.C. Jones, Use of numerical models to determine the effectiveness of anti-vibration systems for railways, *Proceedings of the Institution of Civil Engineers, Transport* 105 (1994) 43–51.
[26] C.J.C. Jones, J.R. Block, Prediction of ground vibration from freight trains, *Journal of Sound and Vibration* 193 (1996) 205–213.
[27] C.J.C. Jones, X. Sheng, M. Petyt, Simulations of ground vibration from a moving harmonic load on a railway track, *Journal of Sound and Vibration* 231 (2000) 739–751.
[28] X. Sheng, C.J.C. Jones, D.J. Thompson, A theoretical study on the influence of the track on train-induced ground vibration, *Journal of Sound and Vibration* 272 (2004) 909–936.
[29] X. Sheng, C.J.C. Jones, D.J. Thompson, A theoretical model for ground vibration from trains generated by vertical track irregularities, *Journal of Sound and Vibration* 272 (2004) 937–965.
[30] X. Sheng, C.J.C. Jones, D.J. Thompson, A comparison of a theoretical model for quasi-statically and dynamically induced environmental vibration from trains with measurements, *Journal of Sound and Vibration* 267 (2003) 621–635.
[31] G. Lombaert, G. Degrande, J. Kogut, S. François, W. Haegeman, L. Karl, An experimental validation of a numerical model for railway induced vibrations at different levels, in: *CD-ROM Proceedings of the Eigth International Workshop on Railway Noise (IWRN8)*, Buxton, Derbyshire, UK, 2004.
[32] Y. Luo, H. Yin, C. Hua, The dynamic response of railway ballast to the action of trains moving at different speeds, *Proceedings of the IMechE, Part F: Journal of Rail and Rapid Transit* 210 (1996) 95–101.
[33] J. Sadeghi, R. Kohoutek, Analytical modelling of railway track system, *Journal of the Rail Track Association Australia* (1995) 20–26.
[34] C. Esveld, J. van't Zand, P.N. Scheepmaker, A.S.J. Suiker, Dynamic behaviour of railway track, *Rail Engineering International Edition* (1996) 17–20.
[35] T. Triantafyllidis, B. Prange, Mitgeführte Biegelinie beim Hochgeschwindigkeitszug "ICE"—Teil I: Theoretische Grundlagen [Live deflection line of the railway track caused by the high speed train "ICE"—part I: theoretical model], *Archive of Applied Mechanics* 64 (1994) 154–168.
[36] T. Triantafyllidis, B. Prange, Mitgeführte Biegelinie beim Hochgeschwindigkeitszug "ICE"—Teil II: Vergleich zwischen theoretischen und experimentellen Ergebnissen [Live deflection line of the railway track caused by the high speed train "ICE"—part II: comparison between theoretical and experimental results], *Archive of Applied Mechanics* 64 (1994) 169–179.
[37] L. Auersch, Zur erschütterungsmindernden Wirkung von Schichten im Boden [On the vibration reduction effects of layers in the soil], in: N. Chouw, G. Schmid (Eds.), *Wave Propagation and Reduction of Vibrations—Wave '94*, Berg-Verlag, Bochum, Germany, 1994, pp. 189–200.
[38] C. Bode, R. Hirschauer, S.A. Savidis, Soil-structure interaction in the time domain using halfspace Green's functions, *Soil Dynamics and Earthquake Engineering* 22 (2002) 283–295.
[39] L. Girardi, P. Recchia, Use of a computational model for assessing dynamical behaviour of a railway structure, *Vehicle System Dynamics Supplement* 20 (1992) 185–194.
[40] H. Takemiya, Traffic induced vibrations and wave propagation, in: N. Chouw, G. Schmid (Eds.), *Wave Propagation and Reduction of Vibrations—Wave '94*, Berg-Verlag, Bochum, Germany, 1994, pp. 151–164.
[41] H. Takemiya, K. Goda, Prediction of ground vibration induced by high-speed train operation, in: C.H. Hansen, G. Vokalek (Eds.), *Proceedings of the Fifth International Congress of Sound and Vibration (ICSV5)*, Vol. 5, International Institute of Acoustics and Vibration, Adelaide, Australia, 1997, pp. 2681–2688.
[42] M. Mohammadi, D.L. Karabalis, Dynamic 3-D soil–railway track interaction by BEM-FEM, *Earthquake Engineering and Structural Dynamics* 24 (1995) 1177–1193.
[43] C. Madhus, A.M. Kaynia, L. Harvik, J.K. Holme, A numerical ground model for railway-induced vibration, in: *Conference Papers—Ground Dynamics and Man-Made Processes*, Institution of Civil Engineers, London, 1997.
[44] A.M. Kaynia, C. Madshus, P. Zackrisson, Ground vibration from high-speed trains: prediction and countermeasure, *Journal of Geotechnical and Geoenvironmental Engineering, ASCE* 126 (2000) 531–537.
[45] J.A. Forrest, Modelling of Ground Vibration from Underground Railways, Ph.D. Thesis, University of Cambridge, 1999.
[46] S.L.D. Ng, Transmission of Ground-borne Vibration from Surface Railway Trains, Ph.D. Thesis, University of Cambridge, 1995.
[47] L. Meirovitch, *Elements of Vibration Analysis*, second ed., McGraw-Hill, New York, 1986.
[48] A.D. Nashif, D.I.G. Jones, J.P. Henderson, *Vibration Damping*, Wiley, New York, 1985.
[49] M. Heckl, G. Hauck, R. Wettschureck, Structure-borne sound and vibration from rail traffic, *Journal of Sound and Vibration* 193 (1996) 175–184.
[50] R.A. Clark, P.A. Dean, J.A. Elkins, S.G. Newton, An investigation into the dynamic effects of railway vehicles running on corrugated rails, *Journal of Mechanical Engineering Science, IMechE* 24 (1982) 65–76.
[51] D.E. Newland, *An Introduction to Random Vibrations, Spectral & Wavelet Analysis*, third ed., Longman, Harlow, Essex, England, 1993.
[52] F. Frederich, Die Gleislage—aus fahrzeugtechnischer Sicht [Effect of track geometry on vehicle performance], *Zeitschrift für Eisenbahnwesen und Vekehrstechnik—Glasers Annalen* 108 (1984) 355–362.